University of Nevada, Reno

Enhanced Extended-Surfaces for Two-Phase Pump-Less Cooling Loops

A dissertation submitted in partial fulfillment of the requirements for the degree of Doctor of Philosophy in Mechanical Engineering

by

Paul J. Laca

Dr. Richard A. Wirtz / Dissertation Advisor

May, 2010

University of Nevada, Reno
Statewide • Worldwide

THE GRADUATE SCHOOL

We recommend that the dissertation
prepared under our supervision by

PAUL J. LACA

entitled

Enhanced Extended-Surfaces
For Two-Phase Pump-Less Cooling Loops

be accepted in partial fulfillment of the
requirements for the degree of

DOCTOR OF PHILOSOPHY

Richard A. Wirtz, Ph.D, Advisor

Jessica Gullbrand, Ph.D., Committee Member

Kwang Kim, Ph.D., Committee Member

Miles Greiner,Ph.D., Committee Member

Jeffrey LaCombe, Ph.D., Committee Member

Vladimir V. Ivanov, Ph.D., Graduate School Representative

Marsha H. Read, Ph. D., Associate Dean, Graduate School

May, 2010

ABSTRACT

Pool boiling experiments are conducted to investigate the heat transfer performance of screen laminate-enhanced extended surfaces in water at reduced pressures. A lamination of fine-filament, wire mesh is an effective surface enhancement for boiling since the surface can be configured to provide a very high density of potential bubble nucleation sites. A coating of copper fine wire screen is bonded to an extended surface (fin). The coating thickness ranged from 0.21mm to 1.3mm. The porosity of the coatings is held constant at 0.43 and the pore hydraulic diameter of the coating varies from 39μm to 172μm. Pool temperatures are held at the saturation temperature for water at pressures of 0.2, 0.3, 0.5 and 1.0atm. A reduction in pressure reduces the boiling performance for all surfaces.

The work began by investigating 4-layer laminates on a fin that has a 1cm^2 base cross section area, a 5deg taper with heights of 1cm and 2/3cm. Boiling performance of a vertical and horizontal fin orientation is investigated. The 4 layer screen laminate enhanced fin with a 10K superheat sustains base heat fluxes of up to 140 W/cm^2 at 1.0atm, and up to 132W/cm^2 at 0.2atm. These extended surfaces outperform screen laminates enhanced plane surface by up to 4 fold. Vertically oriented fins outperform horizontal fins.

The second part of the work was to further investigate screen laminates on the trapezoidal fin. Laminations of 8-layers are found to improve boiling performance over the four layers. Experimental results show that the thin, fine coatings on the fin surfaces enhance the boiling performance. At 0.2atm base heat fluxes in excess of 193W/cm^2 are seen and with moderate superheats of around 10K. A semi-empirical model of the fin is

developed. The model implements a boiling correlation from a plane enhanced surface. Assessments of fin aspect ratio and taper are conducted using the model. Larger aspect ratios improve fin performance. The effects of the taper are negligible.

The last part of the work was to investigate the boiling performance from laminations on a wavy fin array. Two surfaces are considered: a 0.75mm thick 4-layer laminate with approximately 4000 pores per cm^2 and a 0.42mm thick 8-layer laminate with approximately 26,000 pores per cm^2. The results show that the 8-layer laminate outperforms the 4-layer laminate. A semi-empirical boiling model is developed. The model predicts the boiling performance of our data within an error of 30%. The model shows that shorter fins improve boiling performance.

ACKNOWLEDGEMENTS

I would like to thank my advisor, Professor Richard Wirtz for his guidance and support throughout this work. His knowledge and insight have been invaluable. I would also like to thank my committee members: Dr. Miles Greiner, Dr. Jessica Gullbrand, Dr. Kwang Kim, Dr. Jeff Lacombe, and Dr. Vladimir Ivanov for their support and interest in my research. Acknowledgement is also due to my family who has supported me throughout my life. I would also like to thank my colleagues Alison Sloan, Sean Penley, Bharath Ganja, and Zhenghui Zhao to which I collaborated with during my research. Finally, I would like to thank Intel Corporation, Physical Technologies Lab, Hillsboro, OR and the Nevada Applied Research Initiative for funding the project.

TABLE OF CONTENTS

LIST OF TABLES

LIST OF FIGURES

Chapter 1

1.1. Introduction

Historically, the power dissipated from a microprocessor has increased with its computing performance. Processor power levels have tracked Moore's Law such that they have doubled every 36 months [1]. Single phase heat transfer is not adequate for the high thermal loads generated. Liquid-vapor phase heat transfer is an attractive alternative that can meet these demands. It has been shown that vapor phase heat transfer, nucleate boiling and liquid phase heat transfer can coexist on an extended surface, thereby increasing the operating superheat beyond that which is normally associated with the critical heat flux condition. [2]

Nucleate pool boiling on enhanced extended surfaces in water at reduced pressures is investigated. Porous surface enhancements will not only increase the heat transfer surface area, but they are important in promoting bubble nucleation. Water is the working fluid in this study due to its high value of latent heat of vaporization and the saturation temperatures at reduced pressures are relevant to cooling electronics [3].

Many surface and area enhancements are proven to improve heat transfer. Haley and Westwater investigated the optimum fin shape in order to obtain nucleate boiling over the entire surface of a fin. They conclude that an annular spine achieves this [2]. McGillis and Carey used a pin fin type array to increase boiling performance at reduced pressures in water. They conclude that smaller fin gaps are most effective; there is a fin height such that performance does not increase; and, fins can increase the Critical Heat Flux (CHF)

[4]. Fins that have surface enhancements may further improve boiling heat transfer as seen by Nakayama et al. [5]. In this case micro fins are attached to the tip of an extended surface which increased boiling heat transfer in a dielectric fluid. Porous coated fins have been investigated by Laca and Wirtz [6] where fins are coated with 4-layers of screen laminates. They show that a relatively large pore size and thick coating improves boiling performance.

Screens were observed to improve boiling heat transfer as early as 1937 when Jacob bonded a screen onto a heated surface [7]. Gerlach and Joshi use screen mesh soldered to the heater surface as an enhancement in pool boiling in flourinert PF5060. They conclude that the unconfined wire mesh improves heat flux and increases CHF [8]. Li and Peterson use screen laminates, similar to those investigated in this paper, on a horizontal surface to increase boiling heat flux [9]. Holland et.al. [10] found that screen laminates as a porous extended surface matrix can reach heat fluxes in excess of $100W/cm^2$ (flow boiling in FC-72). Similar surface coatings investigated by Sloan et.al. [11] and Penley and Wirtz [12] show that 8-layer laminates and smaller pore sizes improve boiling performance. Penley and Wirtz developed a correlation that predicts the boiling Nusselt number in terms of fluid properties, porous geometry, and superheat. This correlation is used as the heat transfer coefficient in the semi empirical model in this work.

Pal and Joshi report high heat fluxes from rectangular grooved copper surfaces at reduced pressures [13]. Copper metal foam and nanostructured copper surfaces are proven to increase boiling performance as shown by Choon et al and Li et al respectively [14, 15].

1.2. Objectives

Develop an area-enhanced extended surface matrix that fundamentally improves nucleate boiling and can be used as a basic ingredient in high heat density thermal management applications. The technology employs laminations of copper-filament screens that form intrinsically effective vapor nucleation sites. These structures can be configured to provide maximum surface area; and, they can be oriented to have a high lateral conductance.

- Chapter 2 • Experimentally characterize screen-laminates in terms of saturated-liquid (water) nucleate boiling.
- Chapter 3 • Develop and verify a semi-empirical extended surface matrix heat transfer model.
- Chapter 4 • Apply this technology to vertical and horizontal orientation, two-phase cooling loops.

This work investigates copper fins enhanced with a 4-layer and an 8-layer screen laminate in saturated pool boiling experiments. The pore sizes of the screens are varied to investigate a pore size that increases the amount of active nucleation sites. Surface enhanced fins are oriented vertical and horizontal and the pressures range from 0.2atm to 1.0atm, which corresponds to saturation temperatures of 60°C to 100°C.

The first two portions of the work assess boiling performance from trapezoidal shaped fins. Chapter 2, which is the first part of the work, assesses the fin with 4-layer screen laminates. Four layers of mesh have been selected as a starting point for multilayered mesh laminates because Li and Peterson, in their experiments with pool boiling on a

horizontal, screen laminate-enhanced surface found multiple layers to be optimal [9]. With these surfaces a coarser mesh improved the boiling performance the greatest.

In the second part of the work, 8-layer laminates are investigated. The increased number of layers in the screen laminates show the boiling performance is further increased as in Sloan et.al. [11] and Penley and Wirtz [12]. The smaller pores of the 8-layer laminates show an increase in boiling performance. Even though the larger pore size of the 4-layers increase enhancement it is shown in subsequent work that the small pores of the 8-layers further increase the boiling performance. Therefore, the performance enhancement of the laminate is dependent on the number of possible nucleation sites (pores / unit area) and lamination thickness. The optimum is found to be 26,000 pores/cm^2 in 8-layers of mesh with a pore hydraulic diameter of 42μm. A 1-D semi-empirical model is developed utilizing a heat transfer coefficient correlation from a plane surface. The model is derived from the fin equation with an empirical heat transfer coefficient based on the correlation from Penley and Wirtz 2010 [12].

The last part of the work investigates the performance of a way-fin array. The surface consists of two fins that are vertically oriented. The object is to have a thicker base to increase conduction along the fin. This results in an increase in fin surface area that is actively boiling to improve overall boiling performance. The performance of the wavy surface showed a 1.2% increase in superheat at 150W/cm^2 over the trapezoid surface at 1.0atm. At 0.2atm the wavy surface showed a decrease in superheat by 10.1% at 108W/cm^2. This shows that the wavy surface increases the performance at reduced pressure. This can be attributed to the increased conduction towards the fin tip. Another difference is that the trapezoidal fin is not enhanced on the fin tip where as the wavy fin

array is enhanced on the entire surface. A 2-D semi-empirical model is developed to predict the boiling performance of the surfaces. The heat transfer coefficient that is applied to the surface is from a plane surface correlation.

1.3. Organization of the Document

This document is the compilation of publications that are developed during the course of the research. Chapter 2 consists of a conference paper titled, "Sub-Atmospheric Pressure Pool Boiling of Water on a Screen Laminate-Enhanced Extended Surface," by Paul Laca and R.A. Wirtz from the 25th Annual Thermal Measurement, Modeling and Management Symposium, San Jose, CA, March 15-19, 2009. Chapter 3 consists of a journal paper to be submitted to the International Journal of Heat and Mass Transfer and is titled, "Numerical Modeling of Sub-Atmospheric Saturated Pool Boiling of Water on a Structured Porous Enhanced Extended Surface." Chapter 4 is a conference paper titled, "Sub-Atmospheric Pressure Pool Boiling of Water on a Screen Laminate-Enhanced, Wavy-Fin Array," and is accepted to the ASME International Mechanical Engineering Congress and Exposition, Vancouver, British Columbia, November 12-18, 2010.

Chapter 2

Sub-Atmospheric Pressure Pool Boiling of Water on a Screen Laminate-Enhanced Extended Surface

2.1. Abstract

Pool boiling experiments are conducted to investigate the heat transfer performance of screen laminate-enhanced extended surfaces in water at reduced pressures. Screen laminations of varying pore hydraulic diameter and specific surface area fine wire screen are bonded to an extended surface (fin). The fins have a 1 cm^2 base cross section area, a 5 deg taper with heights of 1 cm and 2/3 cm. Pool temperatures are held at the saturation temperature for water at pressures of 0.2, 0.3, 0.5 and 1.0atm. Boiling performance of a vertical and horizontal fin orientation is investigated. The 4 layer screen laminate enhanced fin with a 10K superheat sustains base heat fluxes of up to 140 W/cm^2 at 1.0atm, and up to 132 W/cm^2 at 0.2atm. These extended surfaces outperform screen laminates enhanced plane surface by up to 4 fold. A reduction in saturation pressure reduces the boiling performance for all laminates. Vertically oriented fins outperform horizontal fins.

2.2. Introduction

Historically the power dissipated from a microprocessor has increased with its computing performance. Processor power levels have tracked Moore's Law such that they have doubled every 36 months [1]. Single phase heat transfer is not adequate for the

high thermal loads generated. Liquid-vapor phase heat transfer is an attractive alternative that can meet these demands. It has been shown that vapor phase heat transfer, nucleate boiling and liquid phase heat transfer can coexist on an extended surface, thereby increasing the operating superheat beyond that which is normally associated with the burnout condition. [2] Nucleate pool boiling on enhanced extended surfaces in water at reduced pressures is investigated. Fin surface enhancements will not only increase the heat transfer surface area, but they are important in promoting bubble nucleation. Water is the working fluid in this study due to its high value of latent heat of vaporization and its environmentally safe characteristics. Also the saturation temperatures at reduced pressures are relevant to cooling electronics [3].

Many surface and area enhancements are proven to improve heat transfer. Haley and Westwater investigated the optimum fin shape in order to obtain nucleate boiling over the entire surface of a fin. They conclude that an annular spine achieves this [2]. McGillis and Carey used a pin fin type array to increase boiling performance at reduced pressures in water. They conclude that smaller fin gaps are most effective; there is a fin height such that performance does not increase; and, fins can increase the Critical Heat Flux (CHF) [4]. Fins that have surface enhancements may further improve boiling heat transfer as seen by Nakayama et al. In this case micro fins are attached to the tip of an extended surface which increased boiling heat transfer in a dielectric fluid [5].

Screens were observed to improve boiling heat transfer as early as 1937 when Jacob bonded a screen onto a heated surface [7]. Gerlach and Joshi use screen mesh soldered to the heater surface as an enhancement in pool boiling in flourinert PF5060. They conclude that the unconfined wire mesh improves heat flux and increases CHF [8]. Li

and Peterson use screen laminates, similar to those investigated in this paper, on a horizontal surface to increase boiling heat flux [9].

Pal and Joshi report high heat fluxes from rectangular grooved copper surfaces at reduced pressures [13]. Copper metal foam and nanostructured copper surfaces are proven to increase boiling performance as shown by Choon et al and Li et al respectively [14, 15]. This work investigates extended surfaces (fins) enhanced with 4 layer screen laminates in saturated pool boiling experiments. Surface enhanced fins are oriented vertical and horizontal. Pressures range from 0.2 to 1.0atm. with fin heights of 2/3cm and 1 cm.

2.3. Surface Enhancement

A lamination of wire mesh is an effective surface enhancement for nucleate pool boiling. These highly convoluted open cell structures have large specific surface area, and they can be configured to have a wide ranging pore size. Orthogonal plain weave wire mesh properties include the mesh number, M (wire filaments per mm) and wire filament diameter, d (mm). M and d control the porosity, ε and specific surface area, β (1/cm).

Table 2-1 shows values of these properties for laminations of 50, 80 and 145 mesh weaves. The Table shows all laminations having porosity, $\varepsilon = 43\%$. The specific surface

Table 2-1 Plain weave wire mesh properties

M [mm^{-1}](in^{-1})	d [mm] (in)	ε	β [10^2/cm]	D_h [μm]
2.0 (50)	0.23 (0.0090)	0.43	1	172
3.2 (80)	0.14 (0.0055)	0.43	1.65	105
5.7 (145)	0.06 (0.0022)	0.43	4.04	43

area ranges from 100 cm^{-1} to 404 cm^{-1} while the pore hydraulic diameter $D_h = 4\varepsilon/\beta$ ranges from 172μm to 43μm. The goal is to determine the pore size, characterized by the pore hydraulic diameter that will promote bubble nucleation.

In this work, the screen-laminations are cold rolled to achieve a constant value of the porosity. This makes the pore hydraulic diameter only an inverse function of the specific surface area, β. Therefore, thermal performance will be dependent on only the hydraulic diameter and number of layers that make up the lamination. Relatively large hydraulic diameters are chosen because larger pore sizes are known to be more effective at bubble nucleation in water at low pressures [17]. Four layers of mesh have been selected as a starting point for multilayered mesh laminates because Li and Peterson, in their experiments with pool boiling on a horizontal, screen laminate-enhanced surface found multiple layers to be optimal [9].

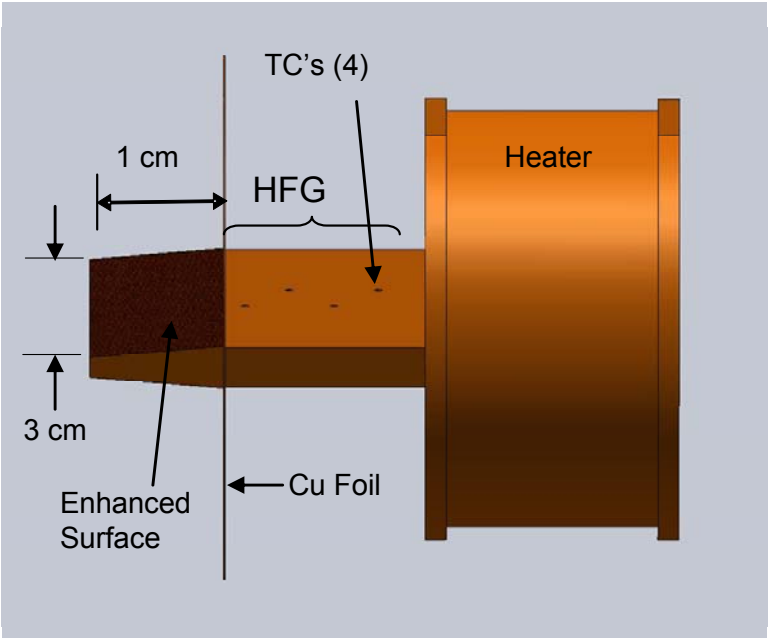

Figure 2-1 Test article assembly

2.4. Extended Surface

In this work, test articles consist of a copper fin with a 5° taper. The fins are 1 cm and 2/3 cm in height with a width of 3 cm and a 1/3 cm base thickness (A_b = 1 cm^2). The fin surfaces are coated with a fine filament screen lamination. Figure 2-1 shows the assembly of the test article. The fin is initially diffusion bonded to a 125 μm thick copper foil base-plate. After this cold rolled copper wire mesh is stacked and diffusion bonded on the fin surfaces. Cold rolling creates flat surfaces that increase bonding area between layers and to the fin surface. Diffusion bonding results in a seamless bond between the copper mesh layers and the fin surface. The copper foil base-plate/enhanced fin assembly is then silver soldered to the tip of a heat flux gauge/heater block (HFG). The heater block supplies the thermal load to the test article while four evenly spaced thermocouples measure the temperature profile of the HFG A linear curve fit of the temperature profile gives the heat flux and the test article base temperature. The HFG is insulated with potted silicone.

The test articles surfaces are identified by, xxMyyyyd-N, where xxM is the mesh number (inch-1), yyyyd is the wire filament diameter, d (in thousandths of an inch) and N is the number of layers in the screen laminate surface.

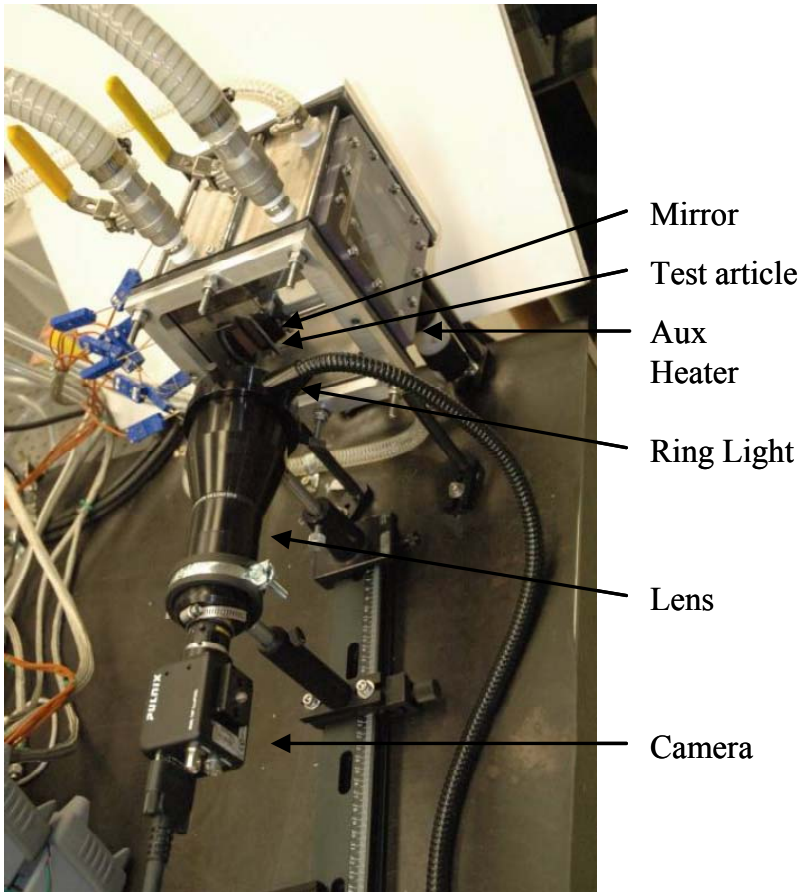

Figure 2-2 Pool boiling test cell.

2.5. Experiment Facility

The test chamber is a 3.5 liter cubical cell with 3 polycarbonate windows for visualization as seen in Fig. 2-2. The test article is mounted into a side wall of the tank with the fin surfaces in vertical orientation. The tank is also rotated to where the test article is mounted from the bottom so the fin is horizontal orientation, with the fin structure pointing up. A vacuum controller maintains system pressure while a pressure transducer verifies the pressure within the test cell. Excess water vapor is condensed and returned to the tank by reflux condensers that are attached between the test cell and the

vacuum controller. Mounted to the test cell is an immersion heater to maintain the pool at saturation temperature. Four type-T thermocouples measure the pool temperature, and two more measure vapor temperature above the pool. These, in conjunction with pool pressure, are used to determine non-condensable gas content. Non-condensable gas content for the experiments reported here is less than 5.0 PPM. Steinke and Kandlikar show that boiling is not affected for gas content below 5 ppm [18].

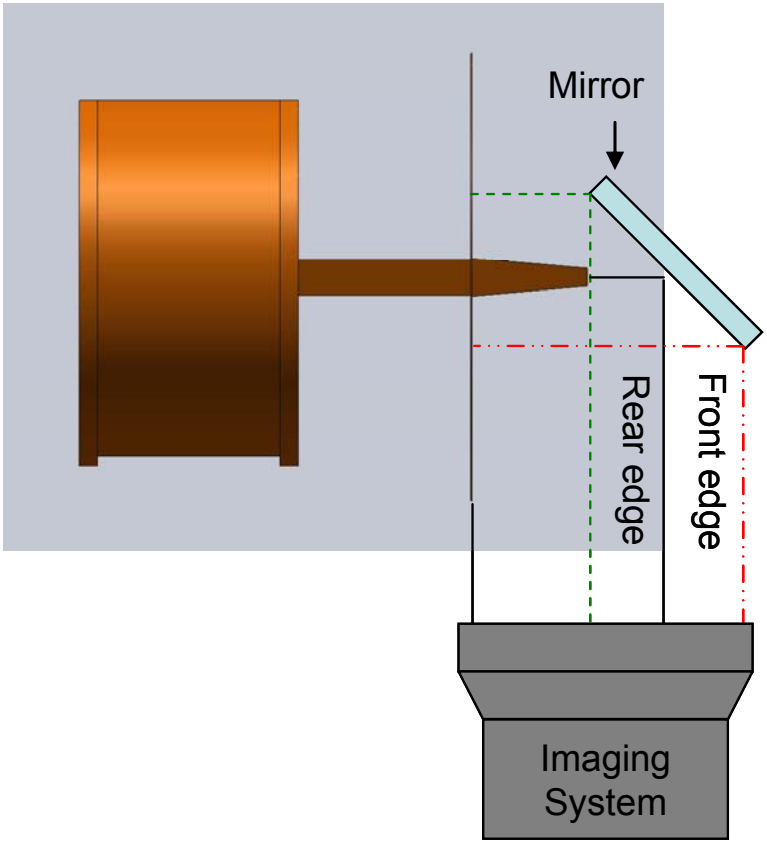

Figure 2-3 Imaging system schematic

A 200 fps camera with a 72 mm telecentric lens records bubble dynamics. A ring light mounted to the lens illuminates the test article. Figure 2-3 is a plan view that shows the orientation of the video system in relation to the test article. As seen in the figure a front view and an edge view of the fin structure are achieved by placing a mirror at 45°

opposite the fin tip. This results in a projected front view with rear and front edge views transposed.

2.6. Experimental Protocol

Fabrication of test articles leaves an oxide layer on the surface and is removed chemically before every experiment. Once the test article is mounted into the tank wall, water is boiled at reduced pressure (0.2atm) for an hour to remove any dissolved air. The pressure is then adjusted for the current experiment and the test article heater is turned on. The auxiliary heater and the test article are left on to increase pool temperature to saturation temperature and to boil-in the screen-laminate surface. After an hour of boiling, data acquisition is initiated.

First dissolved gas content is determined by turning off the heaters, sealing the tank and taking pressure and temperature data for 5 min. Once this is achieved and dissolved gas content is in the correct range (< 5ppm) the boiling experiment starts.

The data acquisition program controls the power levels and acquires data to determine the uncorrected surface heat flux and surface temperature. The power levels are held constant for 5 min before collecting 100 seconds of steady state data and a 4 sec video. The calculated average heat flux and the temperature of the HFG tip are saved to a data file. Raw data from the experiment is also written to a separate data file. The power levels are automatically increased (boiling curve) to a predetermined maximum power level then reduced (cooling curve) until the program is completed.

Videos of boiling are used to assess the effectiveness of the boiling surface. Views of both sides of the fin are seen in vertical oriented experiments and only the front side for horizontal fin orientation. Two views are useful in the determination of the uniformity of boiling between sides. The coalescent frequency of bubbles departing and coalescing as it slides vertically across the surface is also determined.

2.7. Data Reduction and Uncertainty

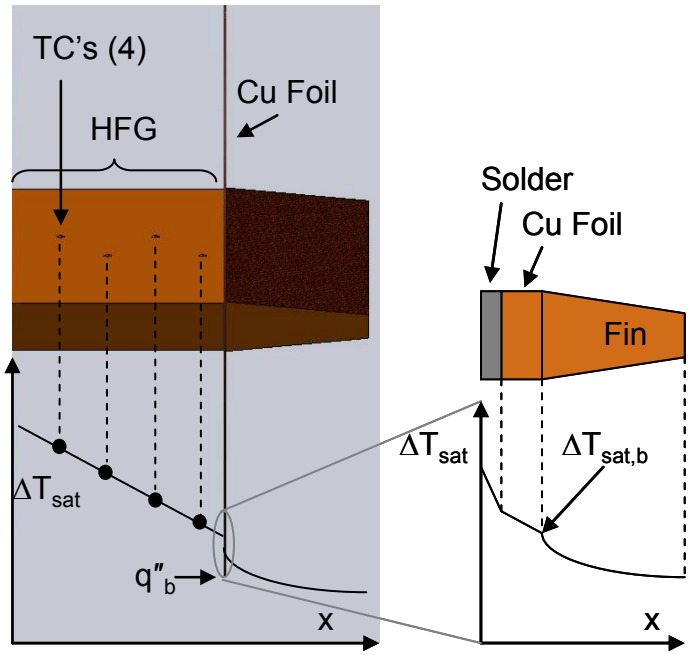

Figure 2-4 Heat flux and superheat

Figure 2-4 shows the placement of the thermocouples in the HFG and a representative temperature distribution. The heat flux and HFG tip temperatures are calculated online using a linear curve fit to the 4 TC's over the 1 cm distance x (cm). The exploded view of the solder joint and copper foil with corresponding temperature drops are seen at the right in Fig. 2-4. Corrections to the heat flux and the fin-base temperature, due to the solder joint and the copper foil are calculated offline. The thermal resistance for the

Table 2-2 Measurement Uncertainty

	Nominal Values	2σ Uncertainty
$\Delta T_{sat,b}$	10 K	2.1 K
q''_b	75 W/cm^2	6.9 W/cm^2
Dissolved Gas	1.0 ppm	0.6 ppm

solder joint between the HFG tip and the copper foil is estimated to be 1.0 [cm·K/W]. The thermal resistance across the copper foil is estimated to be 1.5 [cm·K/W]. Uncertainties in the results are calculated through a Monte Carlo uncertainty propagation simulation. Table 2-2 shows that, assuming 2σ uncertainties in location and temperature of ±0.05mm and ±0.25K, the 2σ uncertainty of the base heat flux is ± 6.9W/cm^2 while the base superheat 2σ uncertainty is ± 2.1 K for nominal values of q''_b = 75W/cm^2 and ΔT_{sat} = 10K. The uncertainty of the dissolved gas for nominal values of 1.0ppm is ±0.6ppm as seen in Table 2-2.

2.8. Results

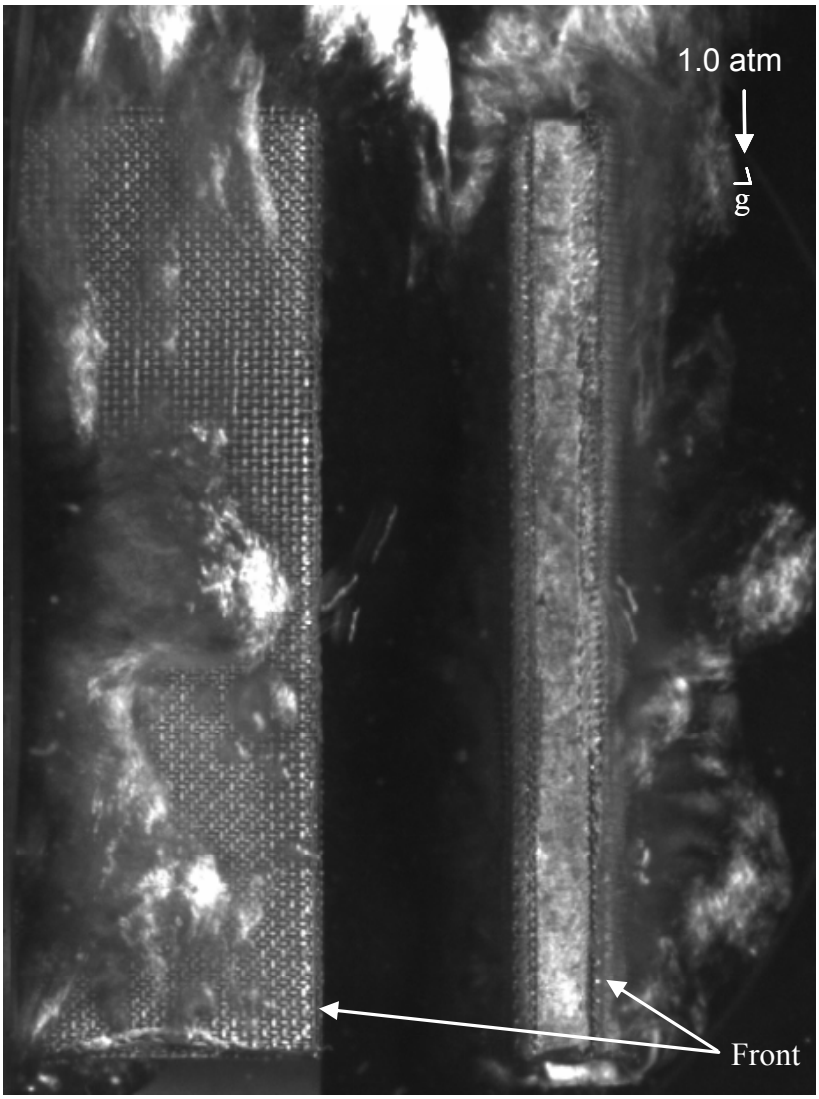

Figure 2-5 80M0055d-4 test article in water. P_{sat} = 1atm, ΔT_{sat} = 8K, q_b'' = 131W/cm^2.

Figure 2-5 shows images of boiling on the 80M0055d-4 test article in vertical orientation. The figure simultaneously shows a projected side view and end view of the tapered fin. Note the location of the "front" surface. This boiling surface has an 8K base superheat and a base heat flux of q''_b = 131W/cm^2. The departing bubbles begin small at the bottom of the surface and coalesce into a large bubble as they travel upward.

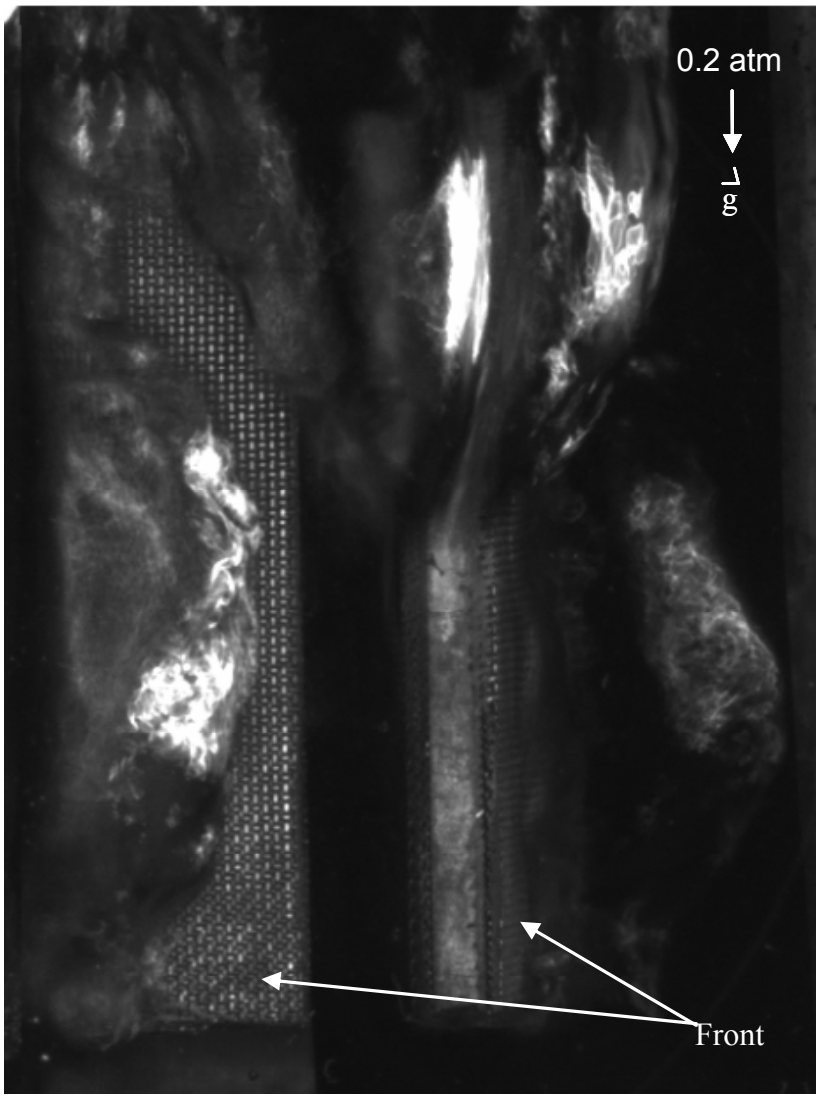

Figure 2-6 80M0055d-4 test article in water. P_{sat} = 0.2atm, ΔT_{sat} = 8K, q_b'' = 95W/cm^2.

Coalescence occurs at a frequency of approximately 13Hz and consequently determination of nucleation site locations is difficult. However, it is observed that the large bubble sweeps over the surface, possibly sweeping up small bubbles that form above it.

The image of boiling on the 80M0055d-4 fin at 0.2atm. shown in Fig. 2-6 has an 8K base superheat with q''_b = 95W/cm^2. The bubble departure size is increased compared to 1.0atm. experiments. The bubbles begin at the bottom of the test article and coalesce with

other bubbles as it sweeps upward across the surface. This occurs at a higher frequency of 20Hz.

The majority of the boiling appears to occur near the base of the extended surface throughout the range of superheats for all pressures. This shows that the entire height of the extended surface is not utilized due to the surface superheat decreasing as the boiling

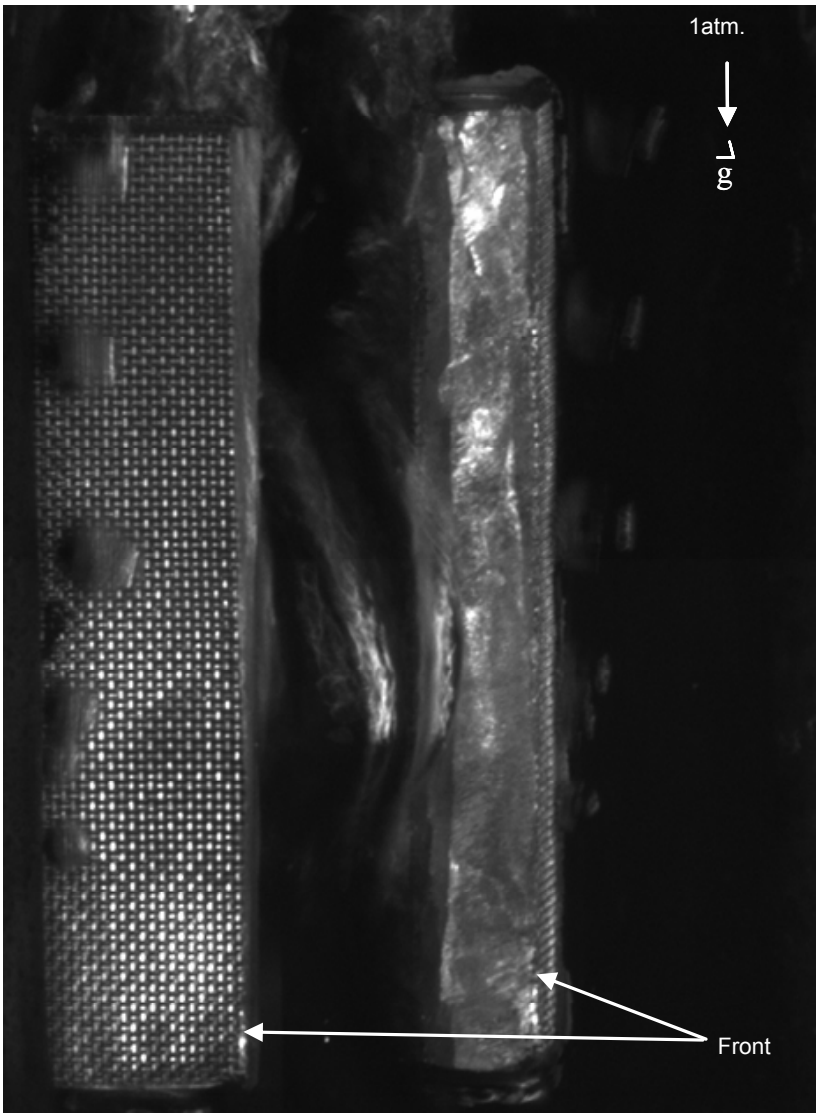

Figure 2-7 Boiling only on rear side of 80M0055d-4, 2/3cm, test article in water at 1.0atm. $\Delta T_{sat,b}$ = 8.5K, q_b'' = 81.9W/cm^2.

extends out from the base, suggesting that shorter fins could be utilized.

Figure 2-7 shows an image of a vertically oriented, 2/3cm height, 80M0055d-4 fin at $\Delta T_{sat,b}$ = 8.5K, q''_b = 81.9W/cm^2. Notice only the back side of the fin is fully boiling. The next higher heat flux for the same surface as Fig. 2-7 is shown in Fig. 2-8 at $\Delta T_{sat,b}$ = 7.8K, q''_b = 100.4W/cm^2. Notice in this image that boiling occurs on both sides of the fin.

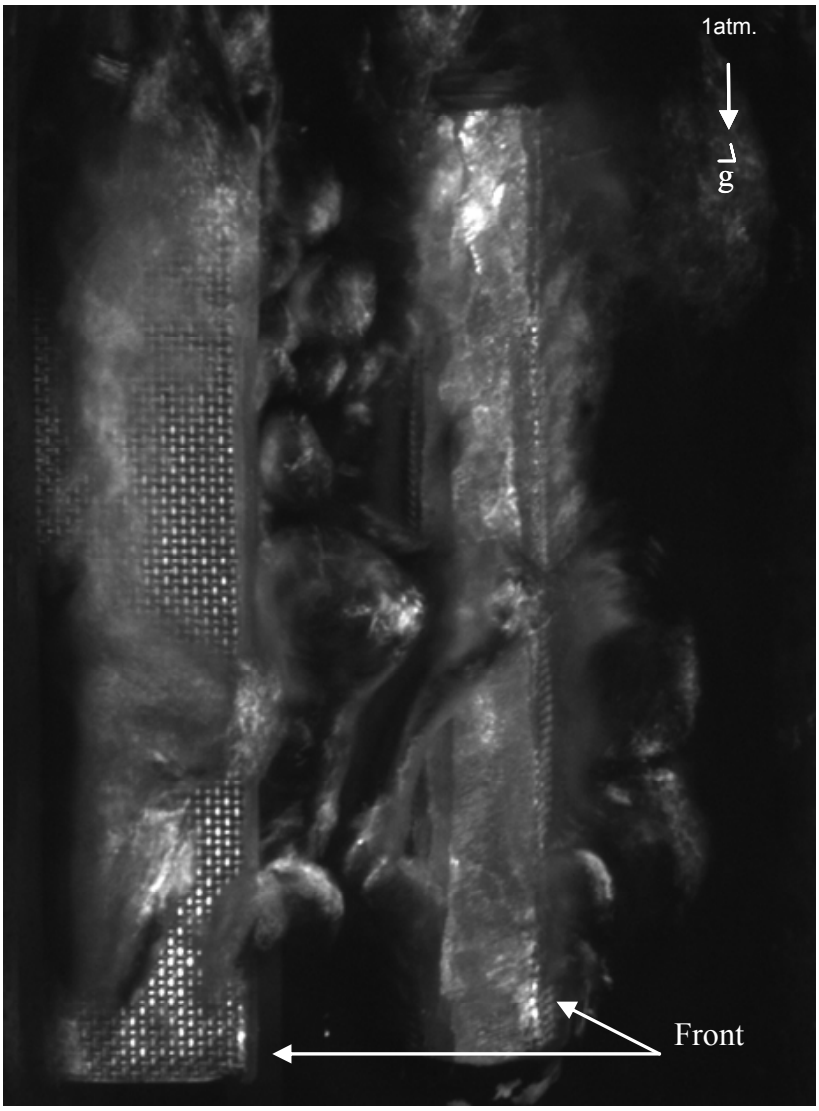

Figure 2-8 ONB for front of 80M0055d-4, 2/3cm, test article in water at 1.0atm is delayed. ΔT_{sat} = 7.8K, q_b'' = 100.4W/cm^2.

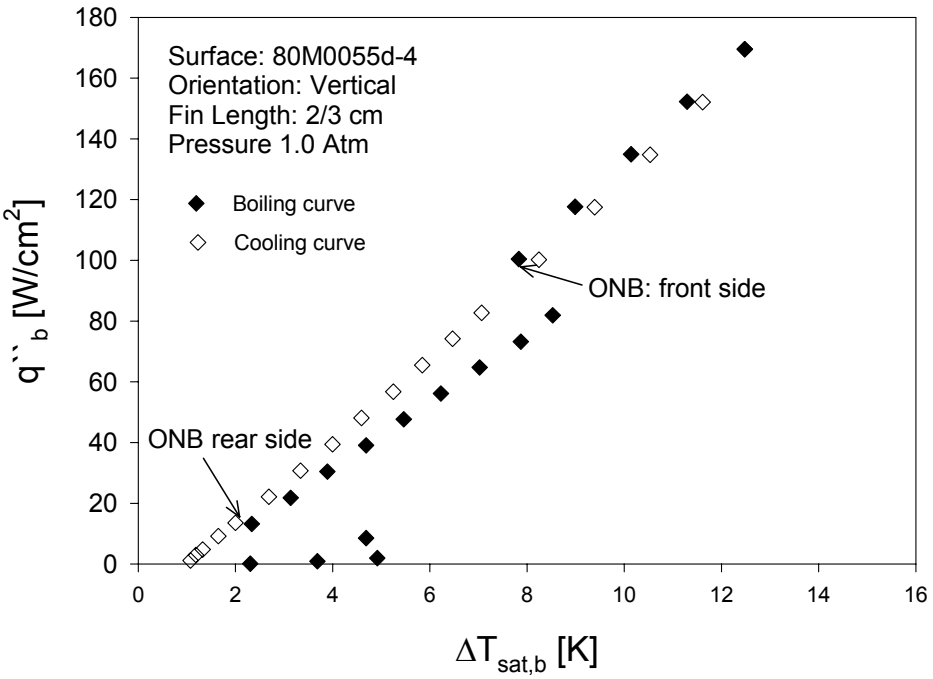

Figure 2-9 Boiling and cooling curves for 80M0055d-4, 2/3cm, test article in water at 1.0atm

The graph of the boiling and cooling curve for the vertical oriented, 2/3cm height, 80M0055d-4 fin is shown in Fig. 2-9. The boiling curve shows discontinuities in the data corresponding to the rear side ONB at $\Delta T_{sat,b}$ = 2.3K, q''_b = 13.2W/cm^2 and ONB of the front side corresponding to $\Delta T_{sat,b}$ = 7.8K, q''_b = 100.4W/cm^2 shown in Fig. 2-8.

This delay of ONB can be attributed to temperature differences between the front and rear surfaces. Due to the discontinuous nature of the boiling curves, only cooling curves are reported in the following results presentation.

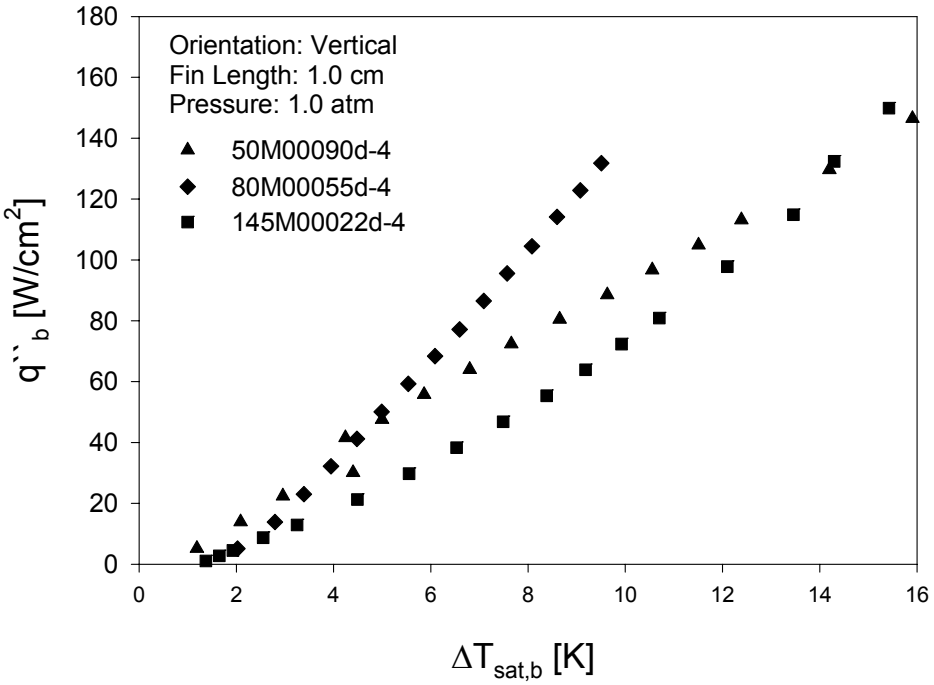

Figure 2-10 Cooling curves from 50M0090d-4, 80M0055d-4 and 145M0022d-4 enhanced fins

Figure 2-10 compares boiling performance at 1.0atm. of 1.0cm height surface enhanced fins with the following surface enhancements: a 4 layer 50 mesh (50M0090d-4), a 4 layer 80 mesh (80M0055d-4) and a 4 layer 145 mesh (145M0022d-4) enhanced surface. The 4 layer 50 mesh surface slightly outperforms the 4 layer 80 mesh surface up to $\Delta T_{sat,b}$ = 4.5K, but the 4 layer 80 mesh out performs 4 layer 50 mesh with increasing base superheat such that at 8K superheat the 80M0055d-4 surface outperforms the 50M0090d-4 by 42%. The 4 layer 145 mesh surface performs equally to the 4 layer 80 mesh surface at low superheats but the 4 layer 80 mesh out performs the 4 layer 145 mesh surface with increasing base superheat such that at 8K superheat the 4 layer 80 mesh surface outperforms the 4 layer 145 mesh by 200%.

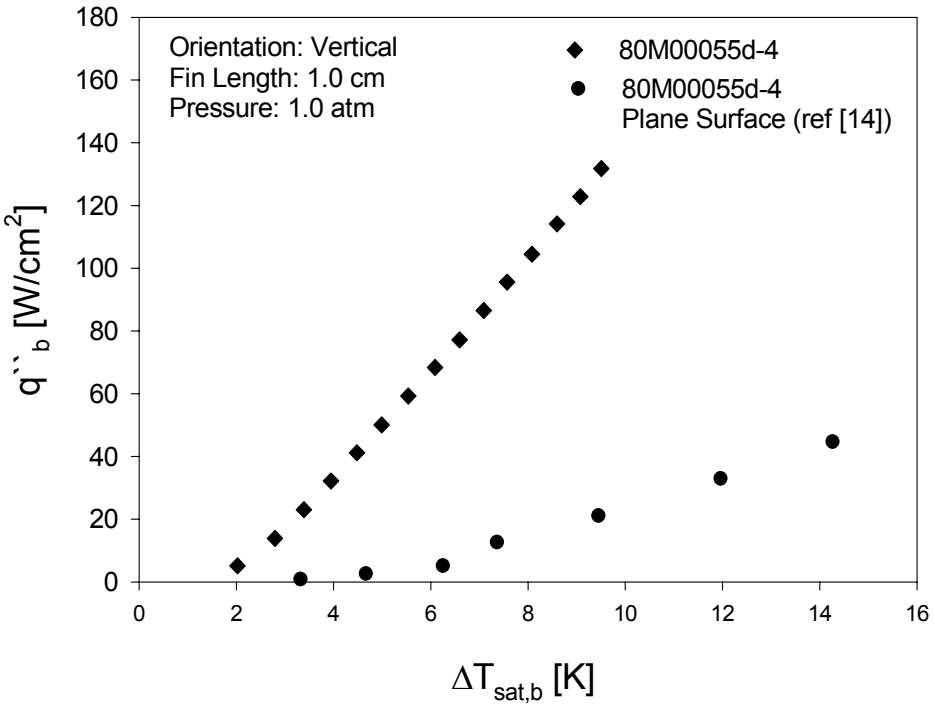

Figure 2-11 Cooling curves from 80M0055d-4 enhanced fin and 80M0055d-4 enhanced plane surface.

Figure 2-11 shows a boiling curve of a 4 layer 80 mesh enhanced plane surface [11] and a cooling curve from a 4 layer 80 mesh enhanced fin. The base superheat of the enhanced fin is compared to the surface superheat of the enhanced plane surface. The 4 layer 80 mesh fin test article at a base superheat, $\Delta T_{sat,b} = 8K$ outperforms the 4 layer 80 mesh plane surface at the same superheat by 400%. This shows that the extended surface utilizes the area enhancement inherent to fins.

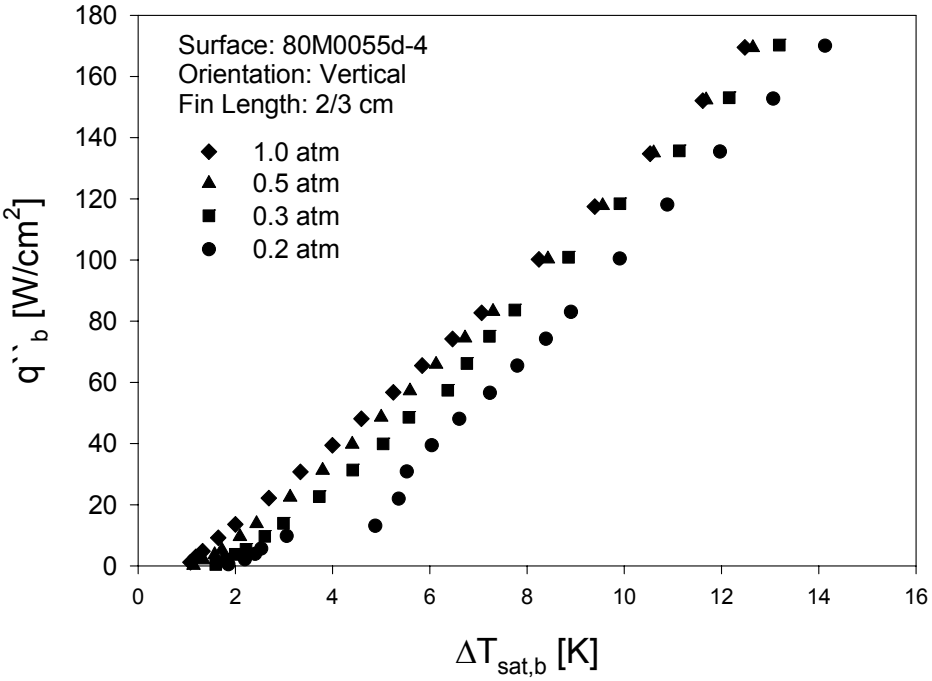

Figure 2-12 Vertical and horizontal test article orientation effects on the 80M0055d-4 1.0cm test article in water at 0.2atm. and 1.0atm.

At reduced pressures the performance of the enhanced extended surface is reduced as seen in Fig. 2-12. Pressures used are 0.2atm. (T_{sat} = 60°C), 0.3atm (T_{sat} = 68°C), 0.5atm (T_{sat} = 82°C) and 1.0atm. (T_{sat} = 100 °C). The 0.5atm data shows a 3% reduction in performance; the 0.3atm. data shows a 10% reduction in performance and the 0.2atm. data shows a 27% reduction in performance relative to the 1.0atm. data. The cooling curves for the 4 pressures show that the base heat flux is approximately linearly proportional to the superheat.

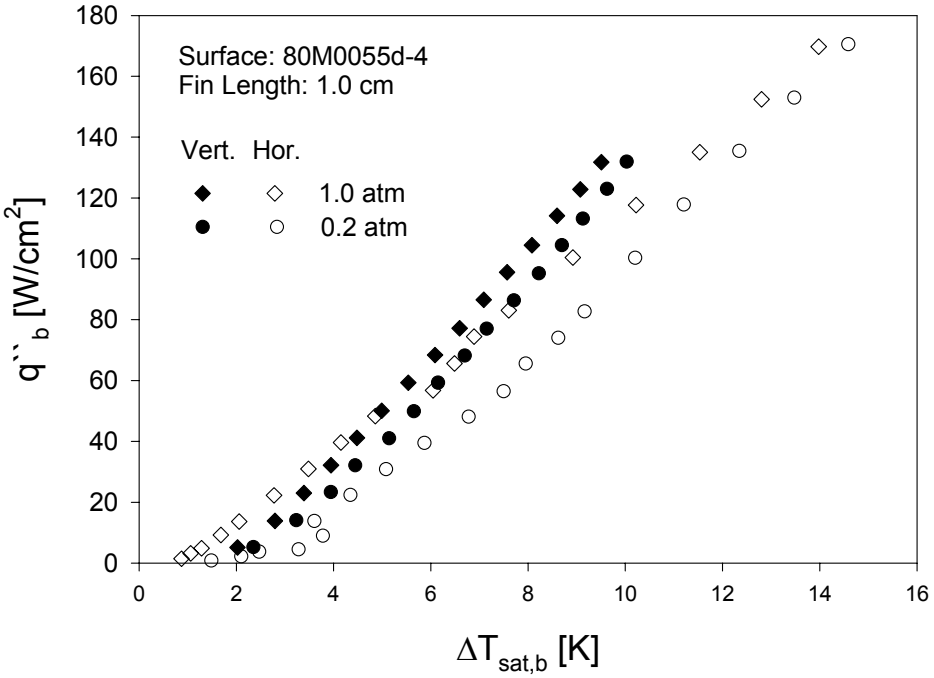

Figure 2-13 Vertical and horizontal test article orientation effects on the 80M0055d-4 1.0cm test article in water at 0.2atm. and 1.0atm.

Figure 2-13 shows the performance dependence on the orientation of an enhanced fin. At 1.0atm the horizontal surface (open diamond symbol) outperforms the vertical surface (closed diamond symbol) up to $\Delta T_{sat,b} = 4.5K$. Then the vertical surface outperforms it at higher superheats. At 0.2atm the vertical orientation (closed circle symbol) outperforms the horizontal test article (open circle symbol) by up to 30%.

The performance advantage of the vertical orientation is attributed to enhancement caused by sliding bubbles as investigated in Bayazit et. al. where the bubble enhances single phase convection as the bubble moves through the water and also because the bubble creates an evaporation microlayer that evaporates and is re-flooded by liquid trapped in front of the rising bubble [20]. The coalescence frequency for the vertical 80M0055d-4 surface is 15Hz at 0.2atm.

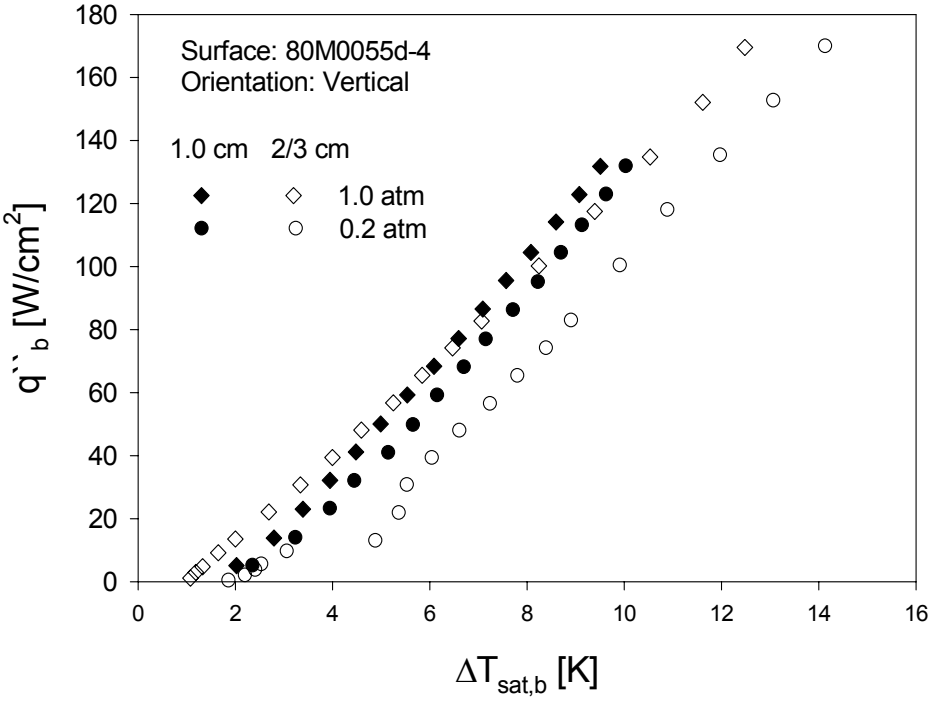

Figure 2-14 Effect of test article height on the 80M0055d-4, vertical test article in water at 0.2atm. and 1.0atm.

The effect of reducing the fin height is shown in Fig. 2-14 where the 1cm tall fin performance is compared to 2/3cm tall fin performance. The figure shows cooling curves for the vertically oriented 4 layer 80 mesh surfaces at 1atm and 0.2atm. At 1atm the 2/3cm tall fin outperforms the 1cm tall fin up to $\Delta T_{sat,b}$ = 6K then the 1cm tall fin outperforms at higher superheats. At 0.2atm the 1cm tall fin outperforms the 2/3cm fin by 12% at $\Delta T_{sat,b}$ = 8K. The added height of the fin increases boiling surface area at higher superheats, but at lower superheats a shorter relatively thicker fin allows for more surface area with active boiling. The reduction in pressure that reduces the boiling performance utilizes the taller fin's boiling surface area that can be in active boiling.

2.9. Conclusions

The effects of changing the pore size of screen laminate surface enhancements, orientation and height of a fin in pool boiling of water at reduced pressures are investigated. The following can be concluded:

- The 4 layer 80 mesh surface enhancement, with a hydraulic diameter in the mid-range of the selected screen laminates produces the greatest increase in boiling performance. This is true for both 1.0atm and 0.2atm. This is attributed to utilization of the area enhancement of the fin and the increased boiling performance due to the screen laminate surfaces.
- Vertically oriented fins outperform horizontally oriented fins for reduced pressures and at higher superheats at 1.0atm. Coalescing bubbles that sweep the fin surface may be the cause for increased heat transfer on the vertically oriented surfaces.
- The 1 cm fin height improved performance at reduced pressure and at 1.0atm, at higher superheats. Although at lower superheats at 1.0atm, the 2/3 cm fin is the leader. This is attributed to more of the fin surface area boiling due to reduced single phase heat transfer of the shorter fin. Coarse meshes augment boiling heat transfer better than fine meshes. This is contrary to Sloan et al's findings [11].

2.10. Appendix A: Nomenclature

A_b = fin base cross section area [cm^2]

β = specific surface area [1/cm]

d = wire filament diameter [mm]

ε = porosity

D_h = pore Hydraulic Diameter [μm]

ΔT_{sat} = Superheat ($T-T_{sat}$) [K]

$\Delta T_{sat,b}$ = Base superheat [K]

M = mesh number (wire filaments per mm)

N = number of mesh layers

q''_b = fin base heat flux [W/cm^2]

T_{sat} = Pool saturation temperature [°C]

x = Distance [cm]

Chapter 3

Experiments and Numerical Modeling of Sub-Atmospheric, Saturated, Pool Boiling of Water on a Structured Porous Enhanced Extended Surface

3.1. Abstract

Nucleate pool boiling experiments in water at sub-atmospheric pressures are conducted on enhanced extended surfaces. Experiments are conducted in water with pressures ranging from 0.2atm to 1.0atm from a vertically oriented copper extended surface (fin). The 5° trapezoid fin is enhanced with laminates of fine filament, copper wire mesh. The coating thickness ranged from 0.42mm to 0.47mm and consists of 8-layer laminates. The porosity of the coatings is held constant at 0.43 and the pore hydraulic diameter of the coating varies from 39μm to 43μm. Experimental results show that the thin, fine coatings on the fin surfaces enhance the boiling performance. At 0.2atm base heat fluxes in excess of 193W/cm^2 are seen and with moderate superheats of around 10K. A semi-empirical model of the fin is developed. The model implements a boiling correlation from a plane enhanced surface. Assessments of fin aspect ratio and taper are conducted using the model. Larger aspect ratios improve fin performance. The effects of the taper are negligible.

3.2. Introduction

Historically, the power dissipated from a microprocessor has increased with its computing performance. Processor power levels have tracked Moore's Law such that they have doubled every 36 months [1]. Single phase heat transfer is not adequate for the high thermal loads generated. Liquid-vapor phase heat transfer is an attractive alternative that can meet these demands. It has been shown that vapor phase heat transfer, nucleate boiling and liquid phase heat transfer can coexist on an extended surface, thereby increasing the operating superheat beyond that which is normally associated with the critical heat flux condition. [2]

Nucleate pool boiling on enhanced extended surfaces in water at reduced pressures is investigated. Porous surface enhancements will not only increase the heat transfer surface area, but they are important in promoting bubble nucleation. Water is the working fluid in this study due to its high value of latent heat of vaporization and the saturation temperatures at reduced pressures are relevant to cooling electronics [3].

Many surface and area enhancements are proven to improve heat transfer. Haley and Westwater investigated the optimum fin shape in order to obtain nucleate boiling over the entire surface of a fin. They conclude that an annular spine achieves this [2]. McGillis and Carey used a pin fin type array to increase boiling performance at reduced pressures in water. They conclude that smaller fin gaps are most effective; there is a fin height such that performance does not increase; and, fins can increase the Critical Heat Flux (CHF) [4]. Fins that have surface enhancements may further improve boiling heat transfer as seen by Nakayama et al. In this case microfins are attached to the tip of an extended

surface which increased boiling heat transfer in a dielectric fluid [5]. Porous coated fins have been investigated by Laca and Wirtz [6] where fins are coated with 4-layers of screen laminates and show that a relatively large pore size and thick coating improves boiling performance.

Screens were observed to improve boiling heat transfer as early as 1937 when Jacob bonded a screen onto a heated surface [7]. Gerlach and Joshi use screen mesh soldered to the heater surface as an enhancement in pool boiling in flourinert PF5060. They conclude that the unconfined wire mesh improves heat flux and increases CHF [8]. Li and Peterson use screen laminates, similar to those investigated in this paper, on a horizontal surface to increase boiling heat flux [9]. Holland et..al. [10] found that screen laminates as a porous extended surface matrix can reach heat fluxes in excess of $100W/cm^2$ (flow boiling in FC-72). Similar surface coatings investigated by Sloan et. al. [11] and Penley and Wirtz [12] show that 8-layer laminates and smaller pore sizes improve boiling performance. Penley and Wirtz developed a correlation that predicts the boiling Nusselt number in terms of fluid properties, porous geometry, and superheat. This correlation is used as the heat transfer coefficient in the semi empirical model in this work.

Pal and Joshi report high heat fluxes from rectangular grooved copper surfaces at reduced pressures [13]. Copper metal foam and nanostructured copper surfaces are proven to increase boiling performance as shown by Choon et al and Li et al respectively [14, 15].

This work investigates fins enhanced with 8-layer screen laminates in saturated pool boiling. Surface enhanced fins with height of 1.0cm are oriented vertical and the

pressures range from 0.2 to 1.0atm. The goal is to determine the screen laminate, characterized by the pore hydraulic diameter, ε, and the number of layers, which will promote bubble nucleation that increases boiling performance.

3.3. Screen Laminate Surfaces

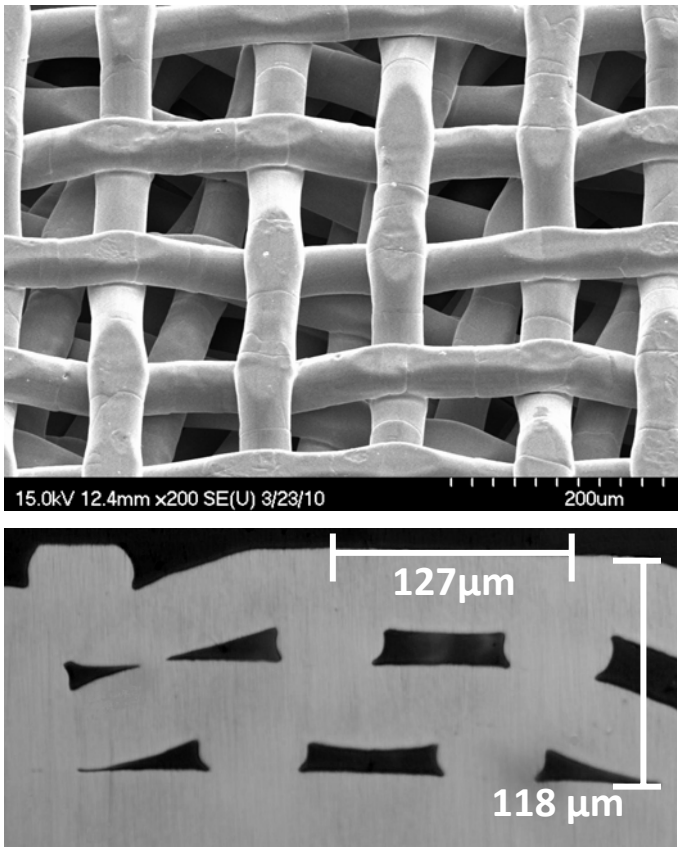

Figure 3-1 Top: SEM of multi-layered laminate. Bottom: Cross section of diffusion bonded, 200 mesh laminate.

A lamination of structured fine wire mesh is a highly convoluted open cell structure having a large specific surface area (β) and a wide ranging pore size. The above image in Fig. 3-1 shows a Scanning Electron Microscope image of a typical mesh laminate. The image on the bottom of Fig.3-1 is a crosssection of a typical bonded lamination.

Orthogonal plain weave wire mesh laminate properties include the mesh number,

M (wire filaments per inch), wire filament diameter (d), number of layers (N), and the lamination thickness, (δ). Table 3-1 shows values of these properties for laminations considered in the experimental and modeling work. The table also shows the porosity, ε, the specific surface area, β, and the pore hydraulic diameter, $D_h = 4\varepsilon/\beta$, where, these parameters are calculated from geometric equations [16]. The last column in Table 3-1 is the surface area enhancement ratio, βδ, that is an important parameter used in the correlation [12]..

Table 3-1 Plain weave wire mesh laminate properties

Mxd		Number of		Porosity	β	D_h	
[mm^{-1}xmm]	[in^{-1}xin]	Layers, N	δ [mm]	ε	[cm^2/cm^3]	[μm]	βδ [-]
3.1x0.140	80x0.0055	4	0.75	0.43	165	105	12
5.7x0.056	145x0.0022	8	0.42	0.43	400	43	17
7.9x0.051	200x0.0020	8	0.47	0.43	440	39	21

In this work, the screen-laminations are cold rolled to achieve a constant value of the porosity. This makes the pore hydraulic diameter only an inverse function of the specific surface area, β. Therefore, thermal performance will be dependent on only the hydraulic diameter and number of layers that make up the lamination. Eight-layer laminates and relatively small hydraulic diameter mesh have been selected for the coatings because Sloan et.al. and Penley and Wirtz [11,12], in their experiments with pool boiling on a vertical, screen laminate-enhanced surface found them to be optimal.

3.4. Extended Surface

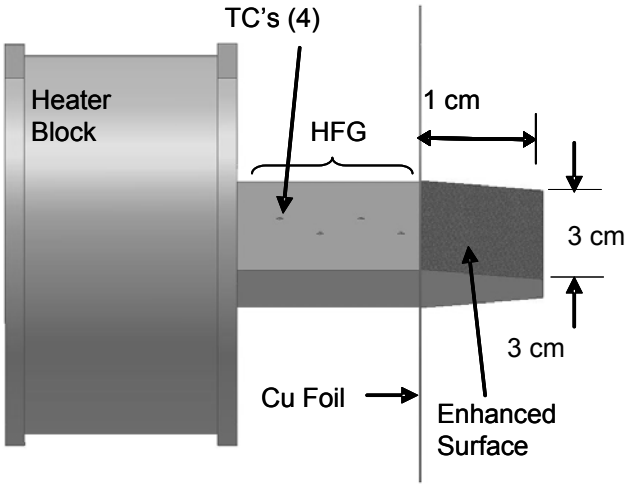

Figure 3-2 Test article assembly

In this work, test articles consist of a copper fin with a 5° taper. The fins are 1 cm in height with a width of 3 cm and a 0.33cm base thickness (A_b = 1 cm^2). The fin surfaces are coated with the fine filament screen lamination. Figure 3-2 shows a perspective view of the assembly of the test article. The fin is initially diffusion bonded to a 0.127mm thick copper foil base-plate. After this cold rolled copper wire mesh is stacked and diffusion bonded on the fin surfaces. A cross section of a 2-layer, 200in^{-1} mesh that is diffusion bonded to copper foil is shown in the bottom image of Fig. 3-1. Cold rolling creates flat surfaces that increase bonding area between layers and to the fin surface. Diffusion bonding results in a seamless bond between the copper mesh layers and the fin surface. The copper foil base-plate/enhanced fin assembly is then silver soldered to the tip of a heat flux gauge/heater block (HFG/HB) assembly. The heater block supplies the thermal load to the test article while four evenly spaced thermocouples measure the

temperature profile of the HFG. A linear curve fit of the temperature profile gives the heat flux and the test article base temperature. The HFG is insulated with potted silicone.

The test articles surfaces are identified by, mmMnnN-ε, where mmM is the mesh number ($inch^{-1}$), nnN is the number of layers on the screen laminate surface, and ε is the porosity.

3.5. Experiment facility

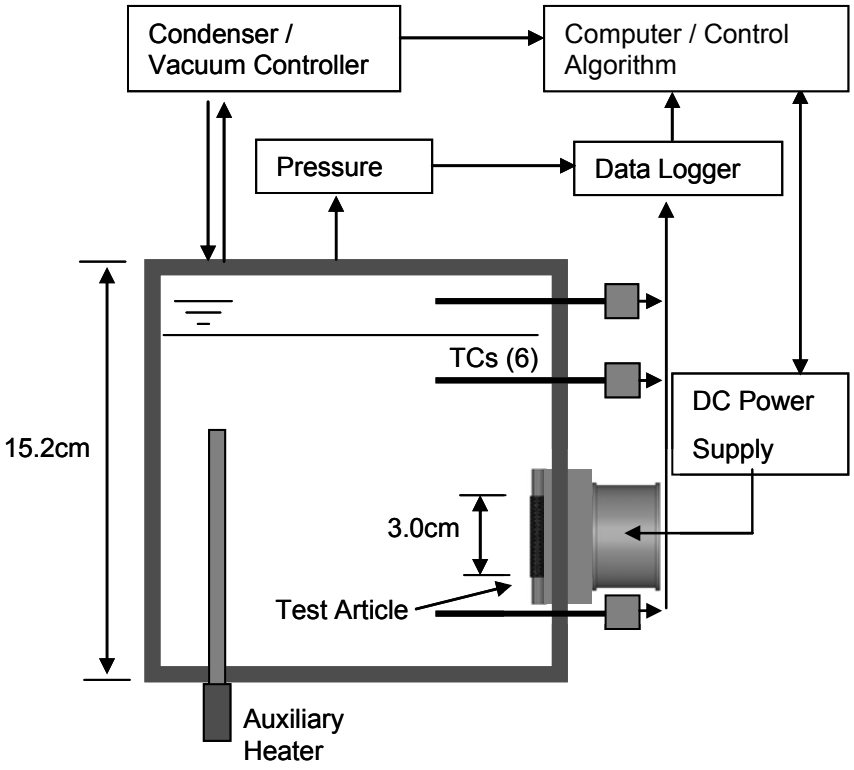

Figure 3-3 Pool boiling test cell

The test chamber is a 3.5 liter cubical cell with 3 polycarbonate windows for visualization as seen in Fig. 3-3. The test article is mounted into a side wall of the tank with the fin surfaces in vertical orientation. A vacuum controller maintains system pressure while a pressure transducer verifies the pressure within the test cell. Excess

water vapor is condensed and returned to the tank by reflux condensers that are attached between the test cell and the vacuum controller. Mounted to the test cell is an immersion heater to maintain the pool at saturation temperature. Four type-T thermocouples measure the pool temperature, and two more measure vapor temperature above the pool. These, in conjunction with pool pressure, are used to determine non-condensable gas content. Non-condensable gas content for the experiments reported here is less than 5.0 PPM.

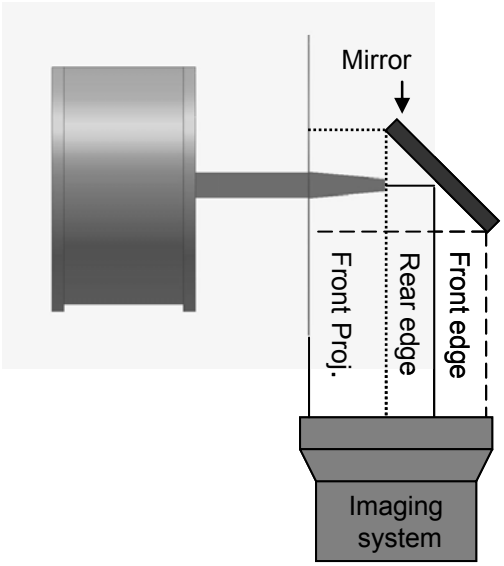

Figure 3-4 Schematic of imaging system

Steinke and Kandlikar show that boiling is not affected for gas content below 5 ppm [18].

A 200 fps camera with a 72 mm telecentric lens records bubble dynamics. A ring light mounted to the lens illuminates the test article. Figure 3-4 is a plan view that shows the orientation of the video system in relation to the test article. As seen in the figure a front view and an edge view of the fin structure are achieved by placing a mirror at 45° opposite the fin tip. The result is a projected front view with rear and front edge views transposed.

3.6. Experiment Protocol

Fabrication of test articles leaves an oxide layer on the surface and is removed chemically before every experiment. Once the test article is mounted into the tank wall, water is boiled at reduced pressure (0.2atm) for an hour to remove any dissolved air. The pressure is then adjusted for the current experiment and the test article heater is turned on. The auxiliary heater and the test article are left on to increase pool temperature to saturation temperature and to boil-in the screen-laminate surface. After an hour of boiling, data acquisition is initiated.

First dissolved gas content is determined by turning off the heaters, sealing the tank and taking pressure and temperature data for 5 min. Once this is achieved and dissolved gas content is in the correct range (< 5ppm) the boiling experiment starts.

The data acquisition program controls the power levels and acquires data to determine the uncorrected surface heat flux and surface temperature. The power levels are held constant for 5 min before collecting 100 seconds of steady state data and a 4 sec video. The calculated average heat flux and the temperature of the HFG tip are saved to a data file. Raw data from the experiment is also written to a separate data file. The power levels are automatically increased (boiling curve) to a predetermined maximum power level then reduced (cooling curve) until the program is completed.

Videos of boiling are used to assess the effectiveness of the boiling surface. Views of both sides of the fin are seen in vertical oriented experiments and are useful in the determination of the uniformity of boiling between sides. The coalescent frequency of

bubbles departing and coalescing as it slides vertically across the surface is also determined.

3.7. Data Reduction and Uncertainty

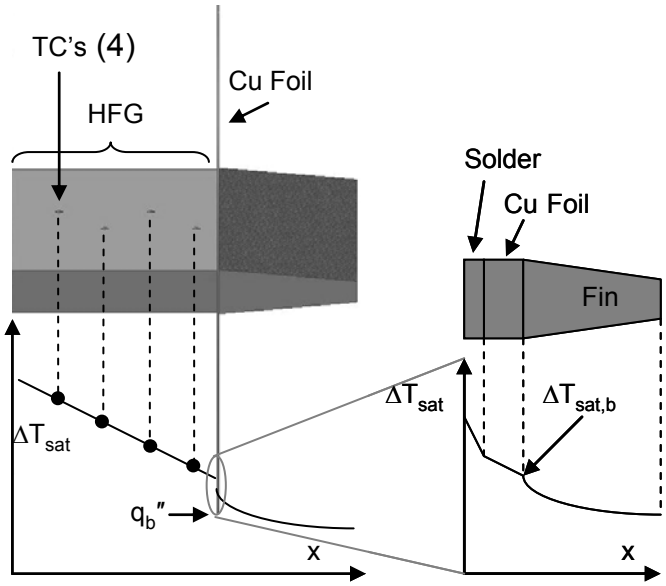

Figure 3-5 Schematic of Heat Flux Gauge

Figure 3-5 shows the placement of the thermocouples in the HFG and a representative temperature distribution. The heat flux and HFG tip temperatures are calculated online using a linear curve fit to the 4 TC's over the 1 cm distance x (cm). The exploded view of the solder joint and copper foil with corresponding temperature drops are seen at the right in Figure 3-5. Corrections to the heat flux and the fin-base temperature, due to the solder joint and the copper foil are calculated offline. The thermal resistance for the solder joint between the HFG tip and the copper foil is estimated to be 1.0 [cm·K/W]. The thermal resistance across the copper foil is estimated to be 1.5 [cm·K/W].

Table 3-2 shows the nominal values of the measurements and the associated 2σ uncertainties (95% confidence interval) in the data for dimensions, temperatures, and

Table 3-2 Measurement Uncertainty

Measured Quantity	Nominal Values	2-σ Uncertainty
linear measurements	0.25 to 6.0 in	±0.005 in
termperature, T	60 to 100°C	±0.25 °C
pressure, P	152 to 760 torr	± 14 torr

Table 3-3 Data Uncertainty

	Nominal Values	2σ Uncertainty
$\Delta T_{sat,b}$	10 K	2.1 K
q''_b	100 W/cm^2	7.8 W/cm^2
Dissolved Gas	1.0 ppm	0.6 ppm

pressure. Uncertainties in the results are calculated through a Monte Carlo uncertainty propagation simulation [19]. The results of the Monte Carlo simulation are listed in Table 3-3 where nominal values for the base superheat, base heat flux and dissolved gas are used to calculate the uncertainty.

3.8. Experimental Results

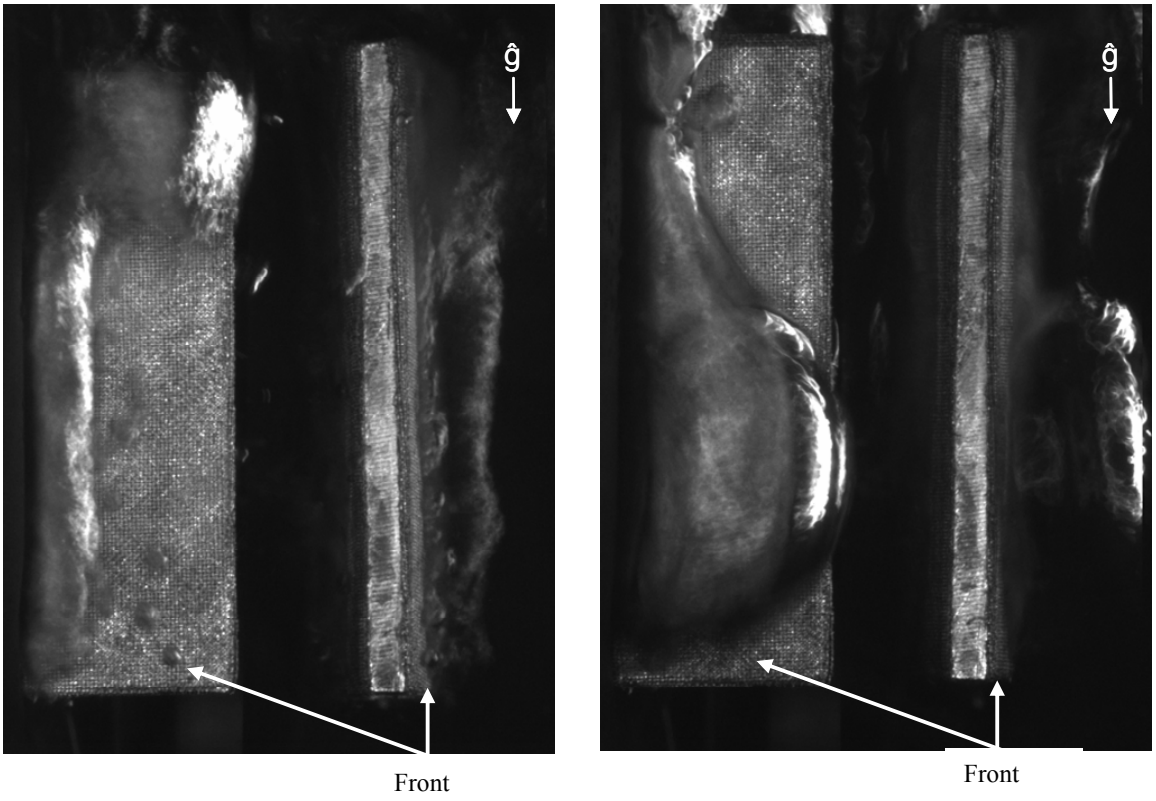

Figure 3-6 145M8N-43 surface, q_b''= 100W/cm^2 left: 1atm ΔTsat,b = 5.9K , right: 0.2atm ΔTsat,b = 8.6K.

Figure 3-6 shows boiling images of the 145M8N-43 surface at 1atm (left) and 0.2atm. (right) at heat flux of $q_b'' = 100 W/cm^2$. The base superheat, $\Delta T_{sat,b}$ for the 1.0atm image is 5.9K and the 0.2atm image $\Delta T_{sat,b}$ = 8.6K. The bubble formation at 1.0atm shows boiling mostly at the base of the fin and that even as the bubbles coalesce they cover only the surface of the fin close to the base. These bubbles coalesce at a frequency of ~25Hz. The 0.2atm image shows that bubbles grow larger and cover much more of the surface. The coalescent frequency is decreased to ~20Hz. This increase in frequency can be explained by the equation from Pioro et al. [21]:

$$f \cdot D_b = 0.6\left[\frac{\sigma g(\rho - \rho_g)}{\rho^2}\right]^{1/4} \tag{3-1}$$

where f is the bubble departure frequency and D_b is the bubble departure diameter. In the equation the bubble departure diameter is inversely proportion to the bubble departure frequency. Since the bubble departure diameter increases for reduced pressures it is expected for the departure frequency to decrease.

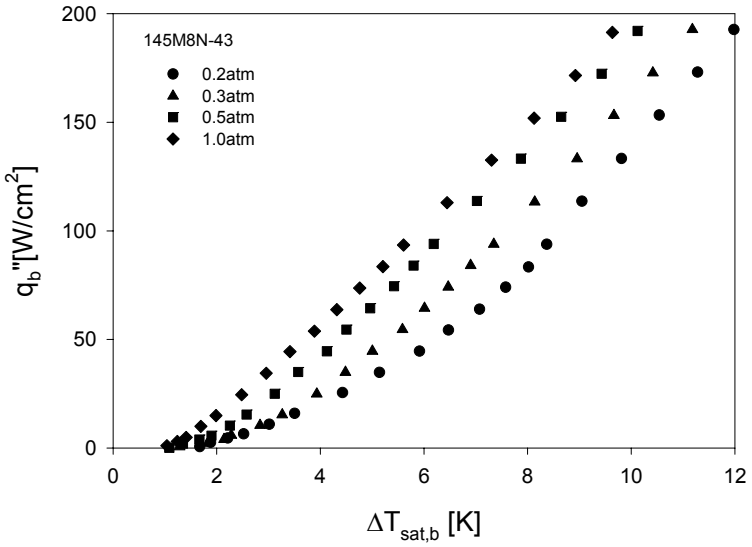

Figure 3-7 Effect of reduced pressure on the 145M8N-43 surface on cooling curves

Figure 3-7 shows the effect on boiling performance of pressure reduction on the 145M8N-43 surface in water. Cooling curves are reported in work due to the delay of onset of nucleate boiling from individual fin surfaces in the array. This is because one surface of the fin array is boiling and the other fin array surface has not sustained a superheat high enough for onset. This delay in onset from one fin surface to the other is also reported by Laca and Wirtz [6]. The 1atm. data shows that at a fin-base heat flux of 150W/cm^2, the superheat is 8.1K. With reduced pressure at the same base heat flux the 0.5atm. superheat is increased by 6.2%, the 0.3atm. by 17.3%, and the 0.2atm. by 28%.

The increase in superheat with decreasing pressure is attributed to the reduction of active nucleation sites and the increased area of vapor coverage. This increase in superheat at reducing pressures is seen in all the surfaces tested.

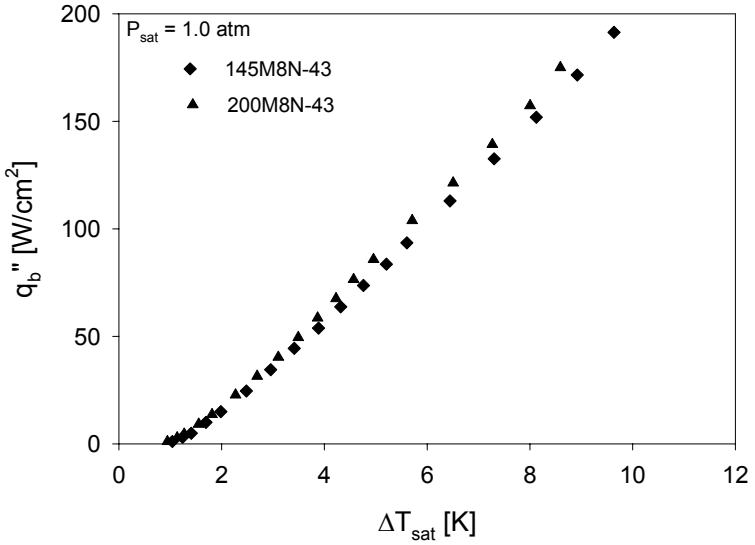

Figure 3-8 Cooling curves at 1.0atm of the 145M8N-43 and 200M8N-43 surface

A comparison of the 2 surfaces at 1.0atm. is shown in Fig. 3-8. The 200M8N-43 is the best performer of these three surfaces and has the smallest pore hydraulic diameter. The smaller pores improve the boiling performance of the surface by increasing the number of nucleation sites. For water at 1.0atm the minimum pore size for bubble ebullition is approximately 7μm. The 200M8N-43 surface is approaching the minimum pore size. The superheat at a 150W/cm^2 for the 200M8N-43 surface is 7.7K. The 145M8N-43 surface superheat at the same heat flux is 5.2% greater than the 200M8N-43 surface. The increase in performance with increase in layer number is attributed to the increase in layer thickness and the increase in the number of pores for bubble ebullition.

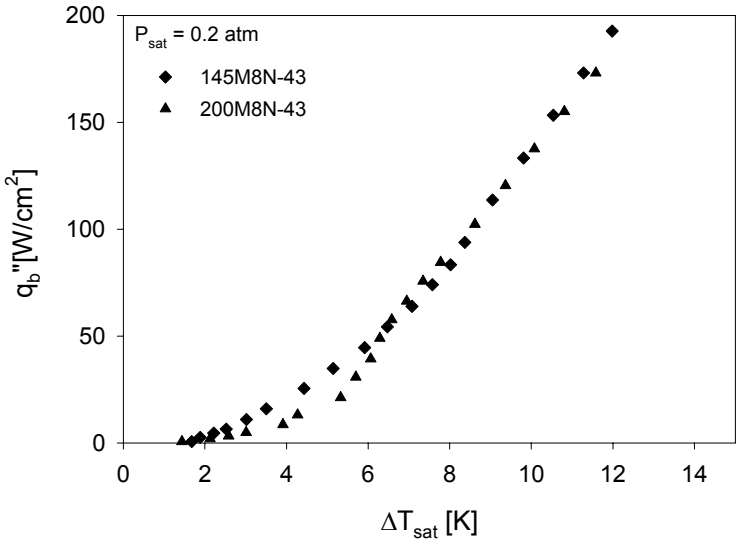

Figure 3-9 Cooling curves at 1.0atm of the 145M8N-43 and 200M8N-43 surface

The 0.2atm performance curves of these surfaces are shown in Fig. 3-9. The 145M8N-8 surface in Fig. 3-9 shows that at 150W/cm^2 the superheat is 10.4K. This figure shows that the superheat for the 200M8N-43 is increased by 1.9% due to the change in operating pressure. The change in pore size has less of an effect on the performance as compared to the 1.0atm data. It is suspected that since a larger area of the fin surface is covered with bubbles sweeping the surface, the increase in number of pores is not as effective.

3.9. Semi-Empirical Model

A 1-D semi-empirical model is developed to predict the boiling performance of the enhanced fin. The equation for the conduction has been derived to include a non-linear boiling heat transfer coefficient from the fin surface.

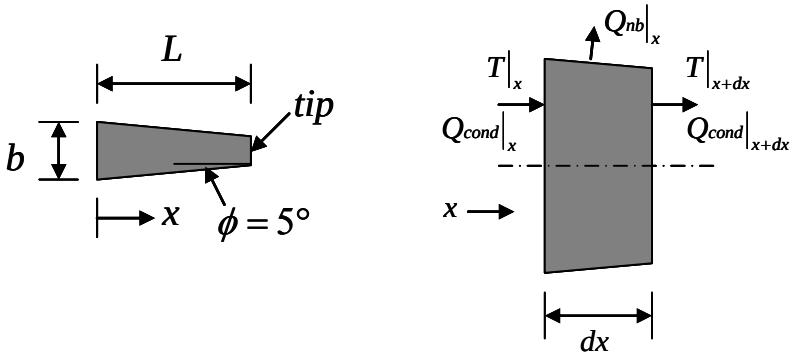

Figure 3-10 Schematic of the fin model

Figure 3-10 shows a sketch of the fin and elemental control volume. The fin has base, b, length, L, and taper angle, ϕ. An Energy Balance on the elemental control volume gives

$$\frac{Q|_x - Q|_{x+dx}}{dx} - \frac{Q_{nb}}{dx} = 0 \tag{3-2}$$

where there is heat conducting through the fin at x and $x+dx$ and nucleate boiling on its surface [24]. Introduction of Fourier's law gives

$$\frac{d^2\theta}{d\eta^2} + \frac{1}{A_{cr}(\eta)}\frac{dA_{cr}}{d\eta}\frac{d\theta}{d\eta} - \frac{dA_s(\eta)}{A_{cr}(\eta)}Bi(\theta) = 0 \tag{3-3}$$

where $\theta = \frac{T - T_{sat}}{T_b - T_{sat}}$ is the non-dimensional temperature, $\eta = \frac{x}{L}$ is the non-dimensional length of the fin, and $Bi(\theta) = \frac{h(\theta)L}{k}$ is the Biot number. The non-dimensional cross sectional area of the trapezoidal fin is given by:

$$A_{cr}(\eta) = \frac{b + \delta_e - \tan(\phi) \cdot \eta L}{L} \tag{3-4}$$

where $\delta_e = \delta(1-\varepsilon)$ is the effective thickness of the porous coating. The non-dimensional surface area of the fin where the boiling occurs is given by the following equation:

$$dA_s(\eta) = \sqrt{\tan(\phi)^2 + 1} \cdot d\eta \tag{3-5}$$

The boundary conditions for the problem are:

$$\theta(\eta = 0) = 1 \text{ and } \left.\frac{d\theta}{d\eta}\right|_{\eta=1} = 0 \tag{3-6}$$

where the temperature at the fin base is known and the fin tip is assumed insulated. The base heat flux is then calculated from the temperature profile using Fourier's law:

$$q_b'' = -\frac{k}{L}\Delta T_{sat,b}\left.\frac{d\theta}{d\eta}\right|_{\eta=0} \tag{3-7}$$

The boiling heat transfer coefficient, $h(\theta)$, that is applied to the fin surface is calculated from the the correlation described in Penley and Wirtz [12]. The correlation is developed from saturated pool boiling data from a vertical plane surface. The experiments are conducted in water and at reduced pressures. The surface consists of

multi-layer screen laminations of copper. The correlation includes the range of laminate layers and mesh properties that are included in this work.

The correlation is given by:

$$\left(\frac{h(\theta)\cdot D_b}{k_f}\right)= 4559\cdot\left(\frac{h(\theta)\cdot D_h}{\Delta T_{sat}\cdot\varepsilon\cdot h_{fg}\cdot\mu_f}\right)^{0.91}\cdot K_{D_{\min}}{}^{0.52} Ja_\rho{}^{0.45}\cdot e^{-0.0025\cdot(\beta\delta-18.8)^2} \tag{3-8}$$

The term on the left hand side of the correlation is the Nusselt number, where D_b is the Cole and Rosenhow [22] bubble departure diameter:

$$D_b = 1.5\times10^{-4}\sqrt{\frac{\sigma}{g(\rho_f-\rho_g)}}\left(\frac{T_{sat}C_p\rho_f}{h_{fg}\rho_g}\right)^{1.25} \tag{3-9}$$

The first term on the right hand side, $\frac{h(\theta)\cdot D_h}{\Delta T_{sat}\cdot\varepsilon\cdot h_{fg}\cdot\mu_f}$, is a pore Reynolds number [22].

The $K_{D_{\min}}$ term is the active nucleation site parameter that describes the volumetric pore density of a porous surface that can serve in nucleation and is given by:

$$K_{D_{\min}} \approx \left(M\cdot D_{\min}\right)^2 \min\left\{N, \frac{k_{ez}}{h(\theta)\cdot\Delta T_{sat}\cdot 2dc_f}\left(T_w - T_{sat}\left(P_p+\frac{4\sigma}{D_h}\right)\right)\right\} \tag{3-10}$$

where, $D_{\min}\equiv\frac{4\sigma}{P_{sat}(T_w)-P_p}$, is the relative size of nucleating bubbles. The minimum of this function is limited on the possible number of nucleation sites that exist for a given number of layers.

$$Ja_\rho = \frac{\Delta T_{sat}C_p\rho_f}{h_{fg}\rho_g} \tag{3-11}$$

is a modified Jakob number. The last term of the correlation defines an optimum of the area enhancement factor, βδ, of the screen lamination. The correlation predicts the

optimum βδ to be 18.8, and is consistent with the current work, where the 145M8N-43 is the optimum surface coating with βδ = 16.9.

Solution Algorithm: The temperature profile, θ, and $\frac{d\theta}{d\eta}$ are the result to the solution to eq. (3-3). It is calculated using an adaptive Runge-Kutta algorithm in conjunction with the shooting method. The heat flux is then calculated from eq. (3-7)

3.10. Model Results

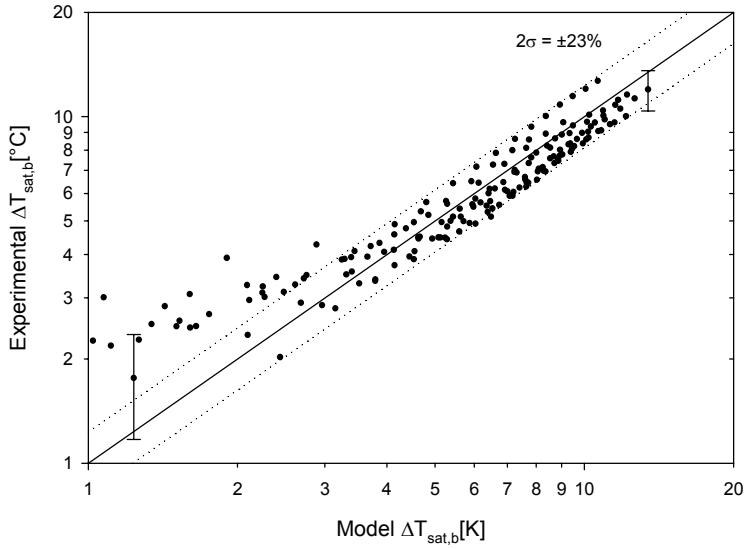

Figure 3-11 Experimental Superheat vs. Model Superheat

Figure 3-11 compares model predictions of fin-base superheat with our experimental measurements. The results of the base superheat from the experiments and the model agree with a 95% confidence-level to ±23% at superheats above 2K. At lower superheats the uncertainty in the experimental data are expected to be high due to the uncertainty analysis and are not included. Uncertainty bars are placed on two points in Fig. 3-11 to show how the uncertainty is large at lower superheats.

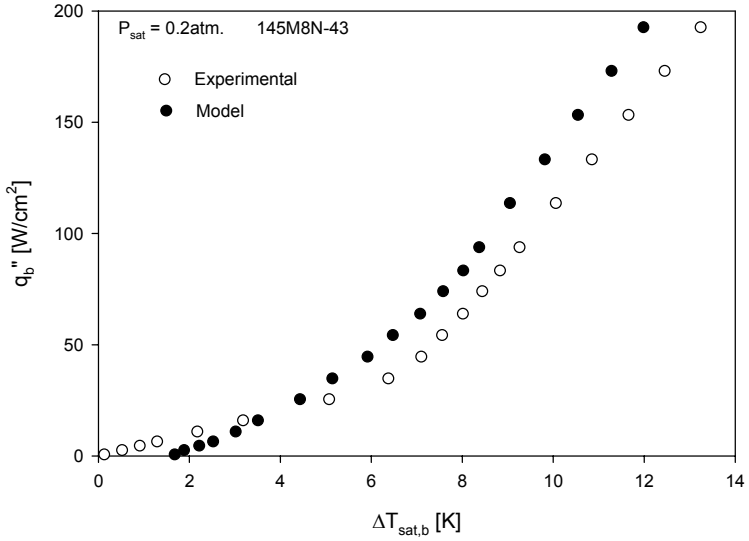

Figure 3-12 Model and experimental comparison for fin at 0.2atm

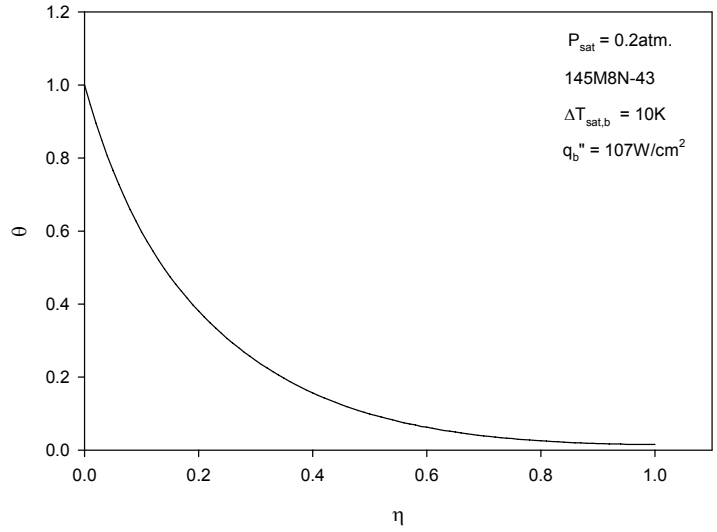

Figure 3-13 Temperature profile for fin at 0.2atm

The results of the model compared with the experimental data for the 145M8N-43 surface is shown in Fig. 3-12. The model calculates lower base superheats for a given base heat flux at higher superheats. There is a 11.6% increase in superheat at a base heat

flux of 100W/cm^2. This is within the uncertainty of the model. The figure also shows that the model over calculates the superheat at low base heat fluxes.

Figure 3-13 shows the temperature profile for a for the 5° taper fin for a pressure of 0.2atm. The superheat is 10K and the base heat flux is 107W/cm^2. The steep slope at the base of the fin shows that the high heat transfer coefficients remove most of the heat near the base of the surface. Only 10% of the base superheat remains at half the fin length. This explains what is observed in the videos where boiling occurs near the base of the fin.

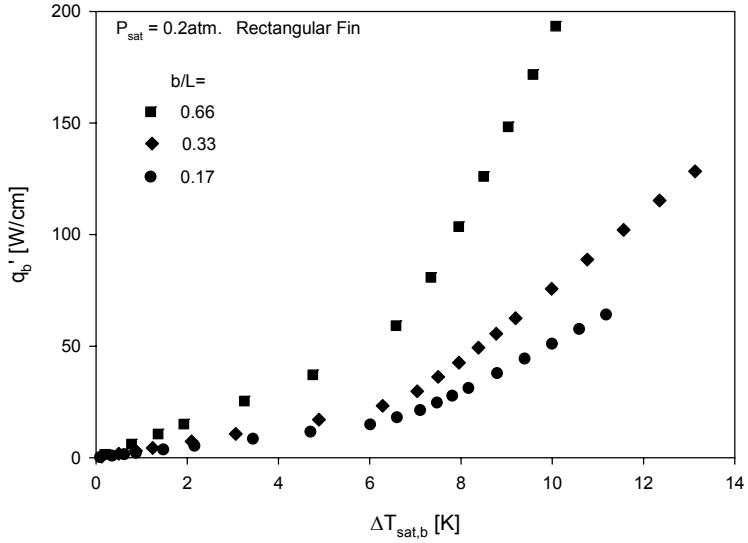

Figure 3-14 Model cooling curves of varying aspect ratio for a rectangular fin at 0.2atm

The model allows performance prediction of various fin profiles. The aspect ratio of the fin is investigated using a rectangular fin profile. Figure 3-14 shows the 0.2atm predicted performance curves for a 145M8N-43 enhanced rectangular fin where the aspect ratios range from b/L = 0.66 to 0.17. The 0.66 aspect ratio has the highest predicted performance. It shows a heat flux per unit width of the fin of $q_b' = 193.3$W/cm

at a superheat of 10K. For the 0.33 aspect ratio fin the superheat is increased by 30.4% at a $q_b' = 100W/cm^2$. Smallest aspect ratio tested, 0.17, shows an 18.2% decrease in superheat over the 0.33 aspect ratio fin at a base heat flux of $60W/cm^2$. It is noted that at larger aspect ratios that the 1-D model becomes less applicable.

The effect of the taper of the 1cm long fin is also investigated using the 0.2atm as a baseline pressure. The performance of a rectangular, 5° taper, and 10° taper fin is predicted and show that the rectangular fin has the highest improvement in performance. The tapered fins lag in performance by less than 2%.

3.11. Conclusions

Pool boiling experiments have been conducted on vertical oriented, screen laminate enhanced, extended surfaces in water at reduced pressures. The pressures ranged from 1.0atm to 0.2atm. The reduction in pressure results in a performance lag with every surface due to the larger bubble departure diameters that cover the surface reducing fluid contact on the coating. The surface coating of fine wire mesh laminates proves to be an effective surface enhancement with the smaller pores enhancing the performance the greatest. In this work the 145M8N-43 surface is the most consistent and shows greatest enhancement for the 0.2atm pressure with superheats of 10.4K at a heat flux of $q_b'' = 150W/cm^2$ At 1.0atm the 200M8N-43 surface shows the greatest enhancement with the superheat of 8.1K at $q_b'' = 150W/cm^2$. Smaller pores lead to an increased number of pores that can be nucleating as in the 1.0atm case. Also small pores can result in a reduction in performance due to the inability of the fluid to permeate the coating and re-flood the cavities near the wall as in the 0.2atm case.

The semi-empirical model is introduced to predict the performance of the enhanced-surface fins. This predicts the performance of the enhanced fin to within ±23% with a 95% confidence level. A parametric study of the effects of the fin aspect ratio and taper is conducted using the model. The aspect ratio of 0.66 shows the greatest improvement in the performance of the fins. The larger aspect ratio improves heat conduction outward from the base. This would result in boiling occurring over a larger area of the surface. The taper of the fins for the 0.33 aspect ratio fin shows that the rectangular fin profile enhances the performance the greatest, while the 5° and 10° taper only lag in performance by less than 2%. The taper in this case has only a minor effect on the performance of the fin.

3.12. Appendix B: Nomenclature

A area [cm^2]

Bi Biot number

d wire filament diameter [mm]

D_h pore hydraulic diameter [μm]

D_{min} minimum bubble diameter due to surface tension-pressure force balance [m]

f bubble departure frequency [Hz]

g gravity

h heat transfer coefficient [W/m^2-K]

h_{fg} latent heat [kJ/kg]

k thermal conductivity [W/m-K]

L	Fin Length [mm]
M	mesh number [m^{-1}]
N	number of layers [-]
n	number of nucleation sites [-]
n''_{pores}	number of pores per unit area [m^{-2}]
P	pressure [atm]
Q	total heat flow [W]
q''	heat flux [W/cm^2]
Re	Reynolds number [-]
ΔT_{sat}	superheat, (T_w-T_{sat}) [K]
T	temperature [K]
x	location [mm]
z	location [mm]

Greek Symbols

β	specific surface area [cm^2/cm^3]
δ	laminate thickness [mm]
ε	porosity [-]
κ	number of pores with sufficient superheat for nucleation [-]
θ	dimensionless temperature $(T-T_{sat})/(T_b-T_{sat})$ [-]
G	fin taper angle °
η	dimensionless distance x/L [-]
μ	dynamic viscosity [$N-s/m^2$]
ρ	density [kg/m^3]

σ	surface tension [N/m]

Subscripts

b	base
c	convection
cond	conduction
cr	cross section
e	effective
ez	effective out-of-plane
f	liquid phase
g	gas phase
h	pore hydraulic diameter
p	pool
s	surface
sat	saturation

Chapter 4

Sub-Atmospheric Pressure Pool Boiling of Water on a Screen Laminate-Enhanced, Wavy-Fin Array

4.1. Abstract

Saturated pool boiling on vertically oriented, copper, wavy-fin surfaces in water at reduced pressures is investigated. A lamination of fine-filament, wire mesh is an effective surface enhancement for boiling since the surface can be configured to provide a very high density of potential bubble nucleation sites. Two surfaces are considered: a 0.75mm thick 4-layer laminate with approximately 4000 pores per cm^2 and a 0.42mm thick 8-layer laminate with approximately 26,000 pores per cm^2. The results show that the 8-layer laminate outperforms the 4-layer laminate. At reduced pressures a reduction in performance is seen for both surfaces. A semi-empirical boiling model is developed. The model predicts the boiling performance of our data within an error of 30%. The model shows that shorter fins improve boiling performance.

4.2. Introduction

Historically, the power dissipated from a microprocessor has increased with its computing performance. Processor power levels have tracked Moore's Law such that they have doubled every 36 months [1]. Single phase heat transfer is not adequate for the high thermal loads generated. Liquid-vapor phase heat transfer is an attractive alternative that can meet these demands. It has been shown that vapor phase heat transfer, nucleate

boiling and liquid phase heat transfer can coexist on an extended surface, thereby increasing the operating superheat beyond that which is normally associated with the critical heat flux condition. [2]

Nucleate pool boiling on enhanced extended surfaces in water at reduced pressures is investigated. Porous surface enhancements will not only increase the heat transfer surface area, but they are important in promoting bubble nucleation. Water is the working fluid in this study due to its high value of latent heat of vaporization and the saturation temperatures at reduced pressures are relevant to cooling electronics [3].

Many surface and area enhancements are proven to improve heat transfer. Haley and Westwater investigated the optimum fin shape in order to obtain nucleate boiling over the entire surface of a fin. They conclude that an annular spine achieves this [2]. McGillis and Carey used a pin fin type array to increase boiling performance at reduced pressures in water. They conclude that smaller fin gaps are most effective; there is a fin height such that performance does not increase; and, fins can increase the Critical Heat Flux (CHF) [4]. Fins that have surface enhancements may further improve boiling heat transfer as seen by Nakayama et al. [5] In this case microfins are attached to the tip of an extended surface which increased boiling heat transfer in a dielectric fluid. Porous coated fins have been investigated by Laca and Wirtz [6] where fins are coated with 4-layers of screen laminates. They show that a relatively large pore size and thick coating improves boiling performance.

Screens were observed to improve boiling heat transfer as early as 1937 when Jacob bonded a screen onto a heated surface [7]. Gerlach and Joshi use screen mesh soldered to the heater surface as an enhancement in pool boiling in flourinert PF5060. They

conclude that the unconfined wire mesh improves heat flux and increases CHF [8]. Li and Peterson use screen laminates, similar to those investigated in this paper, on a horizontal surface to increase boiling heat flux [9]. Holland et.al. [10] found that screen laminates as a porous extended surface matrix can reach heat fluxes in excess of 100W/cm^2 (flow boiling in FC-72). Similar surface coatings investigated by Sloan et. al. [11] and Penley and Wirtz [12] show that 8-layer laminates and smaller pore sizes improve boiling performance. Penley and Wirtz developed a correlation that predicts the boiling Nusselt number in terms of fluid properties, porous geometry, and superheat. This correlation is used as the heat transfer coefficient in the semi empirical model in this work.

Pal and Joshi report high heat fluxes from rectangular grooved copper surfaces at reduced pressures [13]. Copper metal foam and nanostructured copper surfaces are proven to increase boiling performance as shown by Choon et al and Li et al respectively [14, 15].

This work investigates fin arrays enhanced with a 4-layer and an 8-layer screen laminate in saturated pool boiling experiments. Surface enhanced fin arrays with length of 5mm are oriented vertical and the pressures range from 0.2atm to 1.0atm, which corresponds to saturation temperatures of 60°C to 100°C. The goal is to determine the screen laminate, characterized by the pore hydraulic diameter, porosity, and the number of layers, which will promote bubble nucleation that significantly increases boiling performance.

4.3. Screen Laminate Surfaces

These highly convoluted open cell structures have large specific surface area, and they can be configured to have a wide ranging pore size. Orthogonal plain weave wire mesh

Table 4-1 Plain weave wire mesh laminate properties

Mxd		Number of Layers, N	δ [mm]	Porosity ε	β [cm²/cm³]	D_h [μm]	βδ [-]
[mm⁻¹xmm]	[in⁻¹xin]						
3.1x0.140	80x0.0055	4	0.75	0.43	165	105	12
5.7x0.056	145x0.0022	8	0.42	0.43	400	43	17

laminate properties include the mesh number, M (wire filaments per inch), wire filament diameter (d) number of layers (N) and the lamination thickness (δ). Table 4-1 shows values of these properties for laminations considered in the experimental and modeling work. The table also shows the porosity, ε the specific surface area, β and the pore hydraulic diameter, $D_h = 4\varepsilon/\beta$ where, these parameters are calculated from geometric equations [16]. The last column in Table 4-1 is a surface area enhancement ratio, βδ, that is an important parameter used in the correlation [12] used by the modeling in this work. The goal is to determine the screen laminate, characterized by the pore hydraulic diameter and the number of layers which will promote bubble nucleation that increases boiling performance.

In this work, the screen-laminations are cold rolled to achieve a constant value of the porosity. This makes the pore hydraulic diameter only an inverse function of the specific surface area, β. Therefore, thermal performance will be dependent on only the hydraulic diameter and number of layers that make up the lamination. The 4-layer laminate has a relatively large pore hydraulic diameter and is known to promote bubble

nucleation and enhance pool boiling performance [17]. The 8-layer laminate with a relatively small hydraulic diameter mesh is selected for the coatings. Sloan et.al. [11] and Penley and Wirtz [12], in their experiments concluded 8-layers to be optimal.

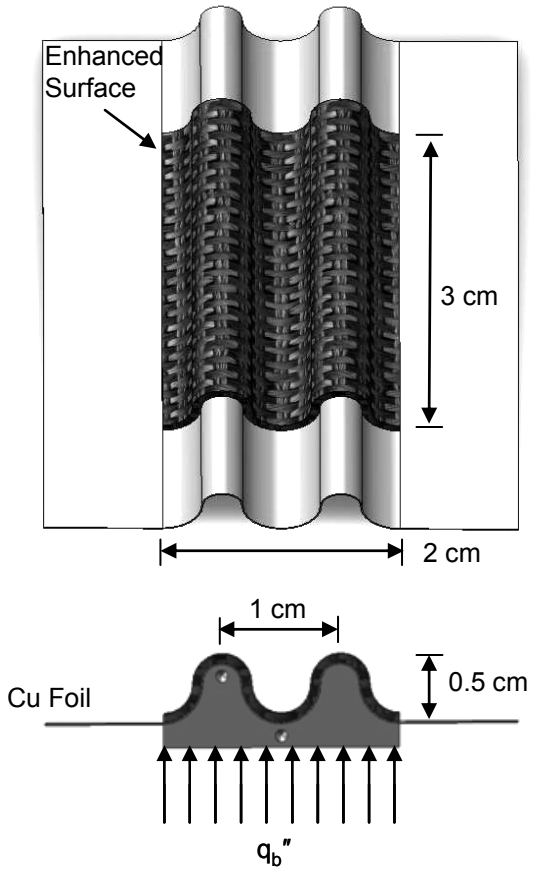

Figure 4-1 Test article assembly

Extended Surface

In this work, test articles consist of copper extended surface array of two "wavy fins". Figure 4-1 shows two views of the test article assembly. The fin is 0.5 cm in length with a width of 3 cm and a 2 cm base thickness (A(base) = 6 cm^2). The radii of curvature of the fins are 0.25 cm. The area enhancement of the wavy fin array compared to a plane

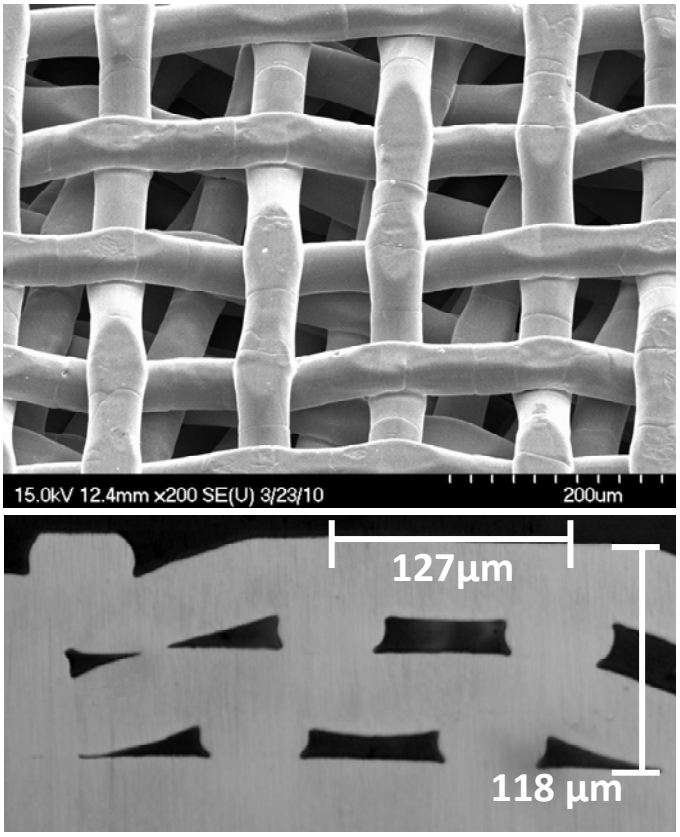

Figure 4-2 Top: SEM of multi-layered laminate. Bottom: Cross section of diffusion bonded, 200 mesh laminate.

surface is 1.5. The wavy fin array surface is coated with a fine filament screen lamination. The top image in Fig. 4-2 shows a Scanning Electron Microscope image of a typical mesh laminate. The bottom of Fig. 4-2 shows a cross section of a 2-layer, $200in^{-1}$ mesh that is diffusion bonded to copper foil. Diffusion bonding results in a seamless bond between the copper mesh layers and the fin surface. The mesh is cold rolled that creates flat surfaces that increase bonding area between layers and to the fin surface

The fin array surface is initially diffusion bonded to a 125 µm thick copper foil. After this, wire mesh is stacked and diffusion bonded on the surface of the copper foil inline with the fin array surface. A thermocouple is soldered to the fin array base to indicate the

base temperature. The fin array base is then silver soldered to a heater and heat flux gauge (HFG). The HFG supplies the thermal load to the test article while four evenly spaced thermocouples indicate the base heat flux. The HFG is then insulated with potted silicone. The heater consists of a copper block heated by a band heater. The test articles surfaces are identified by, mmMnnN-ε, where mmM is the mesh number ($inch^{-1}$), nnN is the number of layers in the screen laminate surface.

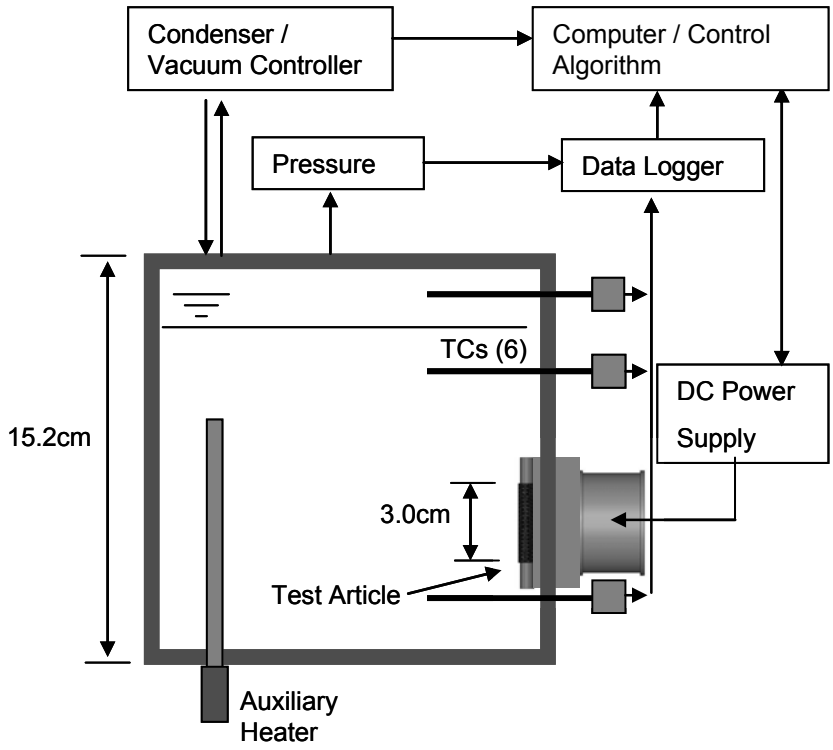

Figure 4-3 Pool boiling test cell.

4.4. Test Facility

The test chamber is a 3.5 liter cubical cell with 3 polycarbonate windows for visualization as seen in Fig. 4-3. The test article is mounted into a side wall of the tank with the fin-array surface in vertical orientation. A vacuum controller maintains system pressure while a pressure transducer verifies the pressure within the test cell. Excess

water vapor is condensed and returned to the tank by reflux condensers that are attached between the test cell and the vacuum controller. Mounted to the test cell is an immersion heater to maintain the pool at saturation temperature. Four type-T thermocouples measure the pool temperature, and two more measure vapor temperature above the pool. These, in conjunction with pool pressure, are used to determine non-condensable gas content. Non-condensable gas content for the experiments reported here is less than 5.0 PPM. Steinke and Kandlikar show that boiling is not affected for gas content below 5 ppm [18].

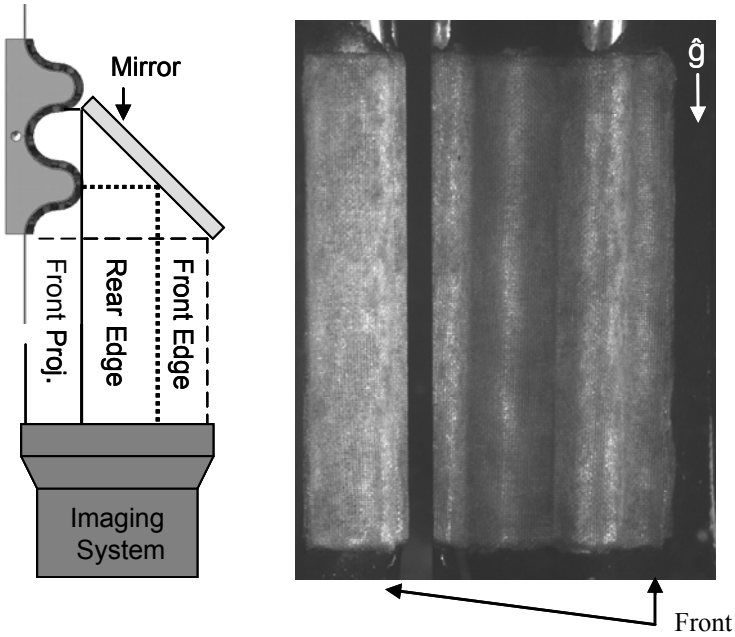

Figure 4-4 Schematic of imaging system

A 200 fps camera with a 72 mm telecentric lens records bubble dynamics. A ring light mounted to the lens illuminates the test article. Figure 4-4 shows a plan view that illustrates the orientation of the video system in relation to the test article. As seen at the left in Fig. 4-4, a front view and an edge view of a partial section of the fin array are achieved by placing a 45° mirror opposite the fin array. The mirror is placed such that the camera captures the maximum area. The image to the right of the schematic is a

typical image in this work where the front projected view is seen in the left of the image. The larger view in the right side of the image shows a partial view of the front edge. It views most of the valley in the fin array. The result is a projected front view with rear and front edge views transposed.

4.5. Experimental Protocol

Fabrication of test articles leaves an oxide layer on the surface and is removed chemically before every experiment. Once the test article is mounted into the tank wall, water is boiled at reduced pressure (0.2atm) for an hour to remove any dissolved air. The pressure is then adjusted for the current experiment and the test article heater is turned on. The auxiliary heater and the test article are left on to increase pool temperature to saturation temperature and to boil-in the screen-laminate surface. After an hour of boiling, data acquisition is initiated.

First dissolved gas content is determined by turning off the heaters, sealing the tank and taking pressure and temperature data for 5 min. Once this is achieved and dissolved gas content is in the correct range (< 5ppm) the boiling experiment starts.

The data acquisition program controls the power levels and acquires data to determine the uncorrected surface heat flux and surface temperature. The power levels are held constant for 5 min before collecting 100 seconds of steady state data and a 4 sec video. The calculated average heat flux and the temperature of the HFG tip are saved to a data file. Raw data from the experiment is also written to a separate data file. The power levels are automatically increased (boiling curve) to a predetermined maximum power level then reduced (cooling curve) until the program is completed.

Videos of boiling are used to assess the effectiveness of the boiling surface. Views of both sides of the fin are seen in vertical oriented experiments and are useful in the determination of the uniformity of boiling between sides. The coalescent frequency of bubbles departing and coalescing as it slides vertically across the surface is also determined.

4.6. Data Reduction and Uncertainty

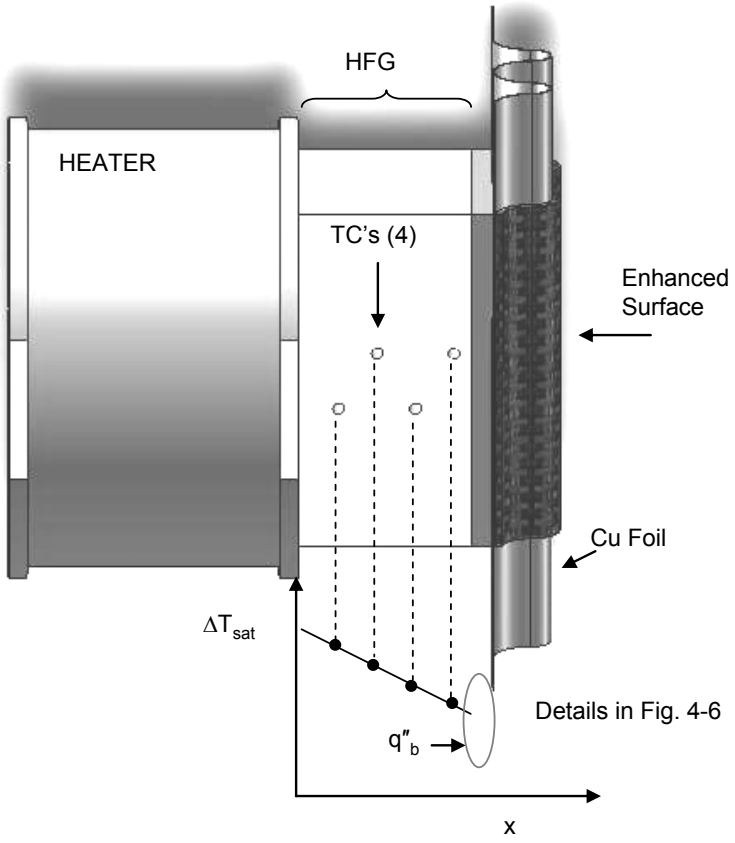

Figure 4-5 Schematic of Heat Flux Gauge

Figure 4-5 shows the placement of the thermocouples in the HFG and a representative temperature distribution. The heat flux and HFG tip temperatures are calculated online using a linear curve fit to the 4 TC's over the 1 cm distance x (cm). The exploded view

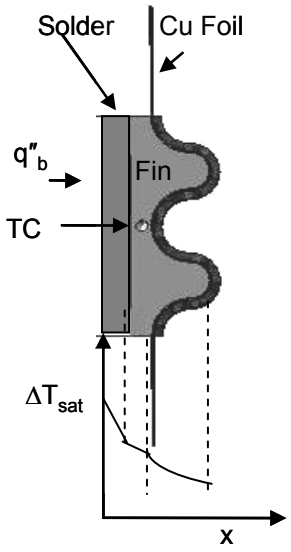

Figure 4-6 Exploded View of the Test Article

of the solder joint and copper foil with corresponding temperature drops are seen in Fig. 4-6. Corrections to the heat flux due to the solder joint and the copper foil are calculated offline. The thermal resistance for the solder joint between the HFG tip and the copper foil is estimated to be 1.0 [cm·K/W]. The thermal resistance across the copper foil is estimated to be 1.5 [cm·K/W]. The fin array base superheat is calculated using the thermocouple that is located 1.127mm away from the base surface. Therefore, the base temperature calculation is independent of the solder joint. Validation thermocouple is soldered to the centerline of a fin 4mm out from the base.

Table 4-2 Measurement Uncertainty

Measured Quantity	Nominal Values	2-σ Uncertainty
linear measurements	0.25 to 6.0 in	±0.005 in
termperature, T	60 to 100°C	±0.25 °C
pressure, P	152 to 760 torr	± 14 torr

Uncertainties in the results are calculated through a Monte Carlo uncertainty propagation simulation [19]. Table 4-2 shows that, assuming 2σ uncertainties in

Table 4-3 Measurement Uncertainty

	Nominal Values	2σ Uncertainty
$\Delta T_{sat,b}$	8°C	0.8°C
q''_b	75 W/cm^2	3.8 W/cm^2
Dissolved Gas	1.0 ppm	0.6 ppm

dimensions and temperature of ±0.005 in and ±0.25K, the 2σ uncertainty of the base heat flux is ± 3.8W/cm^2 while the base superheat 2σ uncertainty is ± 0.8K for nominal values of q''_b = 75W/cm^2 and ΔT_{sat} = 8K. The uncertainty of the dissolved gas for nominal values of 1.0ppm is ±0.6ppm as seen in Table 4-3.

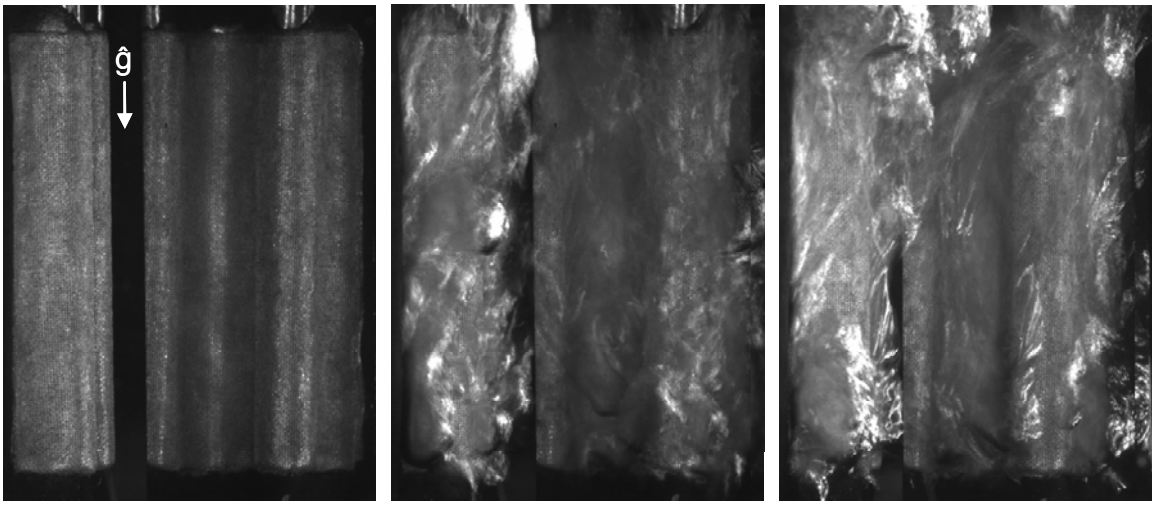

Figure 4-7 Images of 145M8N-43 surface. qb″ = 56W/cm2. a: reference, b: 1.0atm DTsat,b = 4.3K, c: 0.2atm, DTsat,b = 5.6K

4.7. Experimental Results

Figure 4-7 shows images of the 145M8N-43 surface enhanced fin array. Image a: on the left, with no boiling, is a reference of the surface for the images b: and c: on the right. The two images to the right b: and c: show boiling from the fin array at 1.0atm and 0.2atm at a constant heat flux of q_b'' = 56W/cm^2. The respective superheats are a: $\Delta T_{sat,b}$ =

4.3K and b: $\Delta T_{sat,b}$ = 5.6K. The videos of the 1.0atm image show that the bubble departure diameters are on the order of 2mm. The video also shows at high heat fluxes the surface is mostly covered with vapor. The boiling images consist of frames of the video where the bubble ebullition from the surface is seen. Therefore, it is possible to evaluate the surface area with active bubble nucleation. The tip of the fin in view shows that there are many nucleation sites and that there is constant vapor in the valley of the fins. In the image to the right of Fig. 4-7 is the surface boiling at a pressure of 0.2atm. The image shows that most of the boiling is occurring near the base of the fin array and the peak of the fin has very few active nucleation sites. These images show that the increase in superheat at reduced pressures is attributed to the reduction in nucleation sites.

Videos show as the bubbles depart they coalesce and sweep the surface, which, is known to improve performance [20]. The coalescing and departure of the bubbles occur at regular intervals where the frequency is determined by evaluating the videos. The

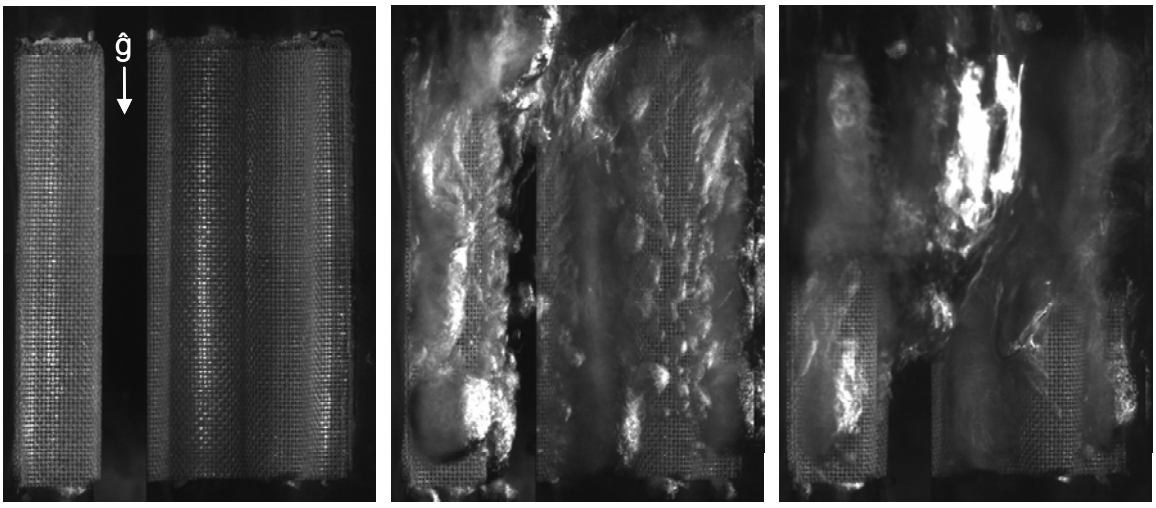

Figure 4-8 Images of 80M4N-43 surface. qb″ = 54W/cm2. a: reference, b: 1.0atm DTsat,b = 4.5K, c: 0.2atm, DTsat,b = 5.6K

coalescent frequencies for the 1.0atm and 0.2atm videos are ~16.4Hz and ~17.3Hz respectively. It is the general case that the coalescence frequency to be higher at reduced pressures. This is because the larger bubbles are more buoyant increasing the rate at which the bubbles leave the surface.

A set of three images are seen for the 80M4N-43 surface in Fig. 4-8. The reference image a: is on the left, b: 1atm image is in the center and c: the 0.2atm image is in the right. The heat flux is constant at $q_b'' = 54W/cm^2$ and the 1.0atm superheat b: is $\Delta T_{sat,b} = 4.5K$ and the superheat at 0.2atm c: is $\Delta T_{sat,b} = 5.6K$. The same results is seen here where the 1.0atm pressure boiling shows many active nucleation sites. The 0.2atm image shows that the boiling occurs very near the array base and shows very few active nucleation sites at the tip.

Comparing the 145M8N-43 and the 80M4N-43 surfaces at both pressures, from Fig. 4-7 and Fig. 4-8, it appears there are more active nucleation sites over the entire surface. This shows that the finer pores and 8-layers of the 145M8N-43 surface increase

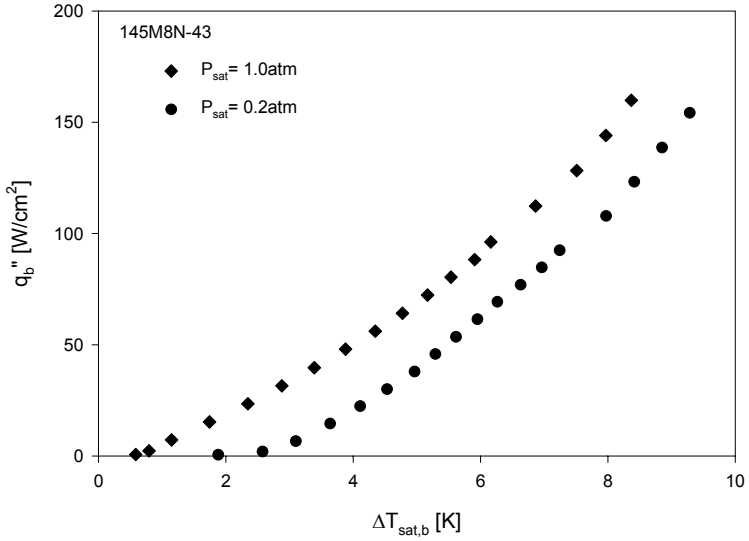

Figure 4-9 Effect of pressure on boiling performance for the 145M8N-43 surface

the overall boiling performance by 5% at a pressure of 1.0atm and $q_b'' = 54 W/cm^2$. This improvement follows the general trends of other work by Sloan et.al. [11].

Figure 4-9 shows the effect on boiling performance of pressure reduction on the 145M8N-43 surface in water. Cooling curves are reported in this work due to the delay of onset of nucleate boiling from individual fin surfaces in the array. This is because one surface of the fin array is boiling and the other fin array surface has not sustained a superheat high enough for onset. This delay in onset from one fin surface to the other is also reported by Laca and Wirtz [6]. The 1atm data shows that at a heat flux of $145 W/cm^2$ the superheat is 8.0K. With reduced pressure at the same base heat flux the 0.2atm superheat is increased by 12.5%. The increase in superheat with decreasing

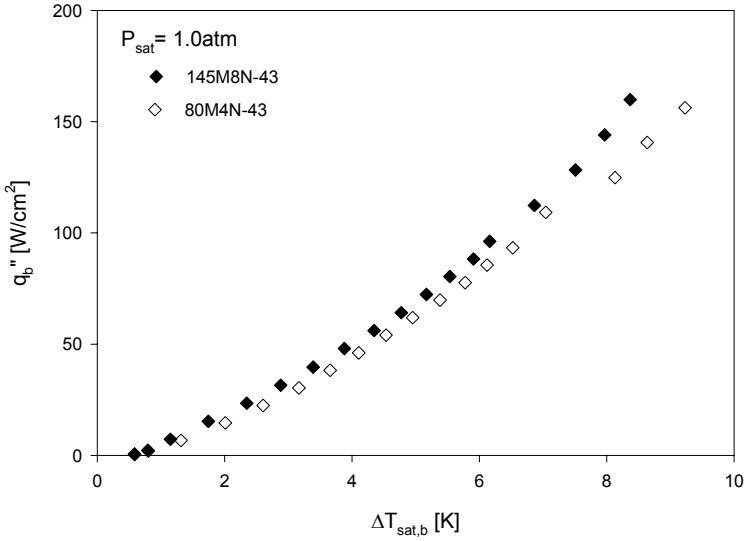

Figure 4-10 1.0atm cooling curves for the 145M8N-43 and 80M4N-43 surfaces

pressure is attributed to the reduction of active nucleation sites. This increase in superheat at reducing pressures is seen in both the surfaces tested.

Figure 4-10 shows the cooling curves for the 145M8N-43 and 80M4N-43 surfaces at 1.0atm. The 145M8N-43 cooling curve at a base heat flux of $145 W/cm^2$ has a base

superheat of 8K. This is a 10% decrease in base superheat over the 80M4N-43 surface. This is attributed to the increase in the area ratio of the 145M8N-43 surface. This trend is also seen in works of Sloan et.al and Penley and Wirtz [11,12]

Cooling curves for the two surfaces at 0.2atm are shown in Fig. 4-11. For the 145M8N-43 at 0.2atm the base heat flux is 109 W/cm^2 at an 8K superheat, which is a 5 percent decrease in base superheat from the 80M4N-43 surface. The decreases in the base superheat are also a result of increased area ratio of the coatings.

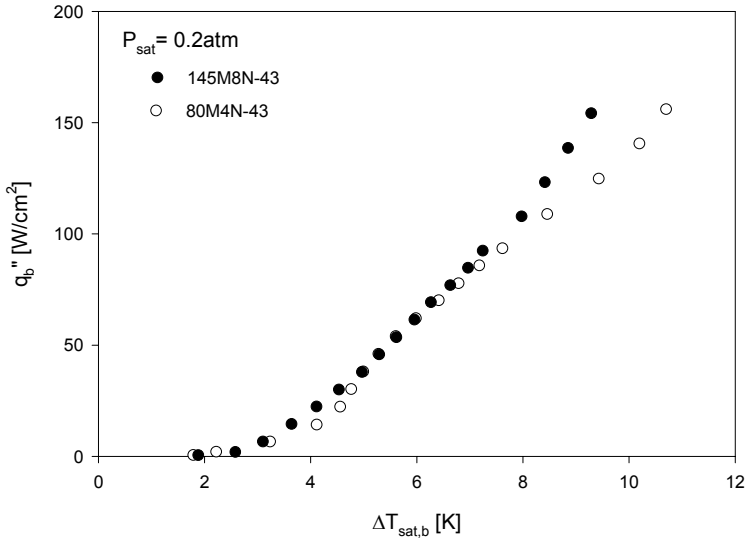

Figure 4-11 0.2atm cooling curves for the 145M8N-43 and 80M4N-43 surfaces

4.8. Semi-Empirical Model

A 2-D semi-empirical model is proposed to calculate the boiling performance using plane surface boiling data as the convection coefficient on the wavy-fin surface. The modeling can be implemented as a design tool to analyze various shaped fins. A commercial finite element code is used to solve the 2-D conduction problem. A symmetrical section of the fin array is used for the geometry. The boundary conditions are the temperature dependent heat flux that is applied as the enhanced surface and a base

temperature that is applied at the base of the fin array. The temperature distribution of the section is calculated and the heat flux at the base is calculated.

The boiling heat transfer coefficient that is applied to the fin surface is calculated from the correlation described in Penley and Wirtz [12]. The correlation is developed from saturated pool boiling data from a vertical plane surface. The experiments are conducted in water and at reduced pressures. The surface consists of multi-layer screen laminations of copper. The correlation includes the range of laminate layers and mesh properties that are included in this work.

The correlation is given by:

$$\left(\frac{h(\theta)\cdot D_b}{k_f}\right) = 4559\cdot\left(\frac{h(\theta)\cdot D_h}{\Delta T_{sat}\cdot\varepsilon\cdot h_{fg}\cdot\mu_f}\right)^{0.91}\cdot K_{D_{\min}}{}^{0.52}\, Ja_\rho{}^{0.45}\cdot e^{-0.0025\cdot(\beta\delta-18.8)^2} \tag{4-1}$$

The term on the left hand side of the correlation is the Nusselt number, where D_b is the Cole and Rosenhow [22] bubble departure diameter:

$$D_b = 1.5\times10^{-4}\sqrt{\frac{\sigma}{g(\rho_f-\rho_g)}}\left(\frac{T_{sat}C_p\rho_f}{h_{fg}\rho_g}\right)^{1.25} \tag{4-2}$$

The first term on the right hand side, $\frac{h(\theta)\cdot D_h}{\Delta T_{sat}\cdot\varepsilon\cdot h_{fg}\cdot\mu_f}$, is a pore Reynolds number [23].

The $K_{D_{\min}}$ term is the active nucleation site parameter that describes the volumetric pore density of a porous surface that can serve in nucleation and is given by:

$$K_{D_{\min}} \approx \left(M\cdot D_{\min}\right)^2 \min\left\{N, \frac{k_{ez}}{h(\theta)\cdot\Delta T_{sat}\cdot 2dc_f}\left(T_w - T_{sat}\left(P_p + \frac{4\sigma}{D_h}\right)\right)\right\} \tag{4-3}$$

where, $D_{\min} \equiv \frac{4\sigma}{P_{sat}(T_w)-P_p}$, is the relative size of nucleating bubbles. The minimum of this function is limited on the possible number of nucleation sites that exist for a given number of layers.

$$Ja_{\rho} = \frac{\Delta T_{sat} C_p \rho_f}{h_{fg} \rho_g} \tag{4-4}$$

is a modified Jakob number. The last term of the correlation defines an optimum of the area enhancement factor, βδ, of the screen lamination. The correlation predicts the optimum βδ to be 18.8, and is consistent with the current work, where the 145M8N-43 is the optimum surface coating with βδ = 16.9.

4.9. Model Results

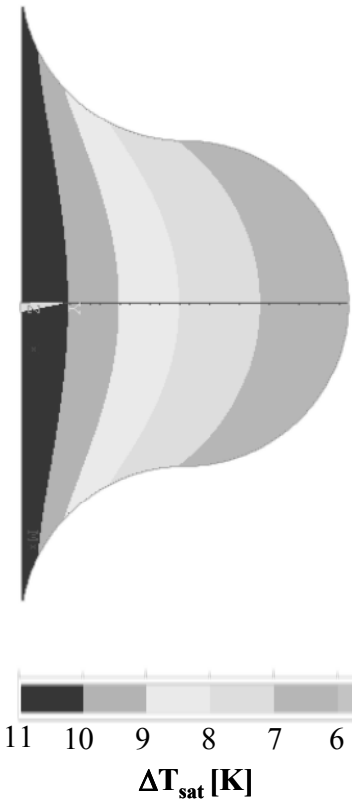

Figure 4-12 0.2atm temperature distribution of L = 5mm fin array

Figure 4-12 shows a contour plot of the temperature distribution for the 145M8N-43 surface at 0.2atm. The base heat flux is 103.1W/cm^2 at a base superheat of 11K. The profiles show curved contours where the temperature at the center of the fin is higher than the surface temperature at a given distance from the fin base. The verification thermocouple 4mm away from the base under predicts the temperature by 45%.

Figure 4-13 shows the results of the model and experimental data for the 145M8N-43 surface at 1.0atm and 0.2atm. The curves show that the model under estimates the experimental performance curves. At 1atm and at a base heat flux of 150W/cm^2 the base superheat is 8K. The model calculates that the base superheat at that heat flux to be 9K,

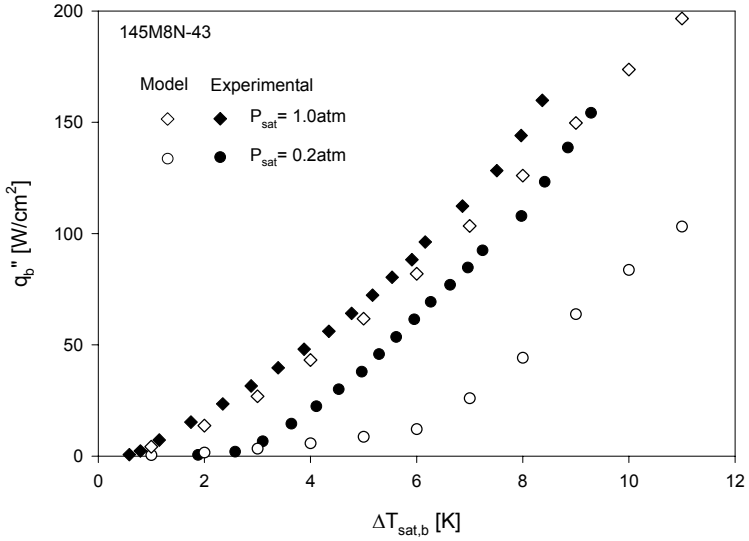

Figure 4-13 1.0atm model boiling curves for the 145M8N-43 surface and fin-array heights of 2.5mm and 5mm

which is a 12.5% increase in superheat. At 0.2atm and a base heat flux of 107.8W/cm2 the base superheat is 7.9K. The model calculates a 37.5% increase in superheat over the experimental data at that heat flux. This performance increase is attributed to the increase in the area ratio of the wavy-fin. The error in the base heat flux of the model is within 30%

The model can be used to assess the effect of the fin array height has on the boiling performance. In this study the correlation data is used as a baseline or fin height of 0mm. The fin heights ranged from 0mm up to 5mm. The radius of curvature is adjusted to maintain the one fin per cm pitch. A 2.5mm fin length array with radii of curvature of 3.125mm and area ratio of 1.2 is evaluated in this investigation. Figure 4-14 shows the results from the model and correlation for the 145M8N-43 surface at 1.0atm. The plane surface outperforms the model of both fin arrays. At a heat flux of 100W/cm^2 the plane surface has a superheat of 4.9K. At the same heat flux the superheat is increased by 37.7% for the 2.5mm fin array and 38.8% increase for the 5mm tall fin array.

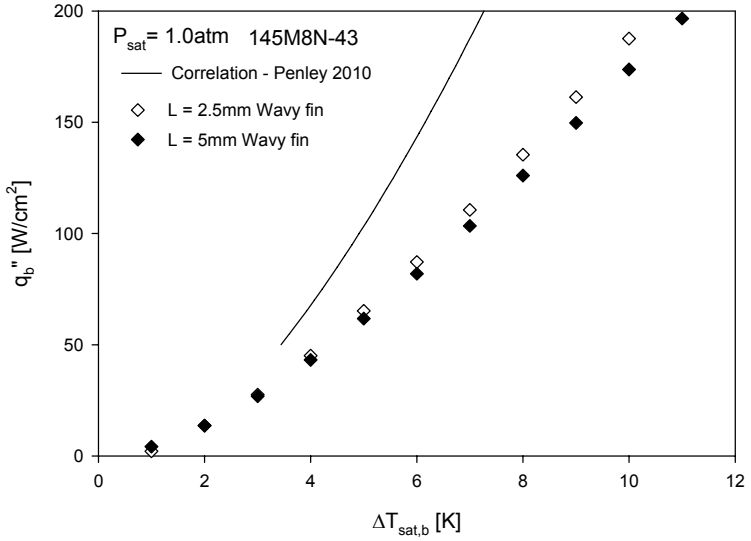

Figure 4-14 Experimental and model boiling curves for the 145M8N-43 surface

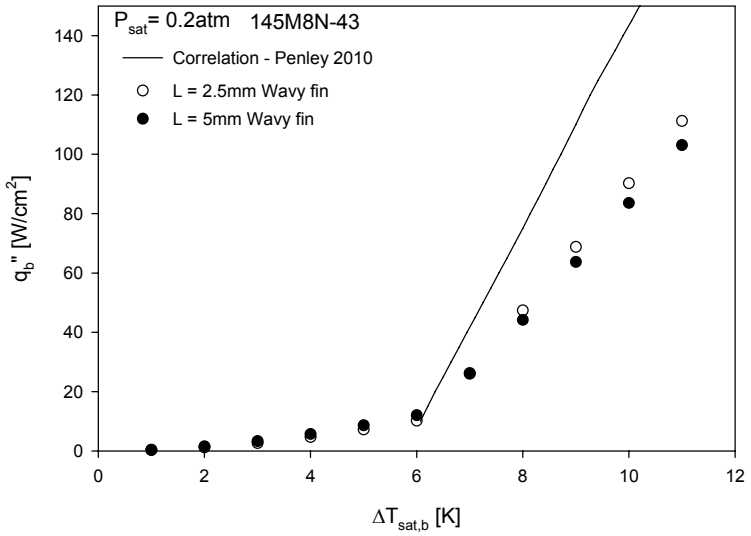

Figure 4-15 0.2atm model boiling curves for the 145M8N-43 surface and fin-array heights of 2.5mm and 5mm

Figure 4-15 shows the effect of fin length for the 145M8N-43 surface at 0.2atm. The figure shows that the plane surface outperforms the fin surface. At 100W/cm^2 the plane surface superheat is 8.7K. The base superheat from the model of the 2.5mm and 5mm tall

fin array are increased by 21% and 24% respectively. The plane surface shows the greatest performance enhancement when compared to the fin array. This shows that as the area ratio of the fin array increases the performance decreases. The temperature profile and results show that the fin effectiveness to be low for the high performance of the plane surface. This is due to the boiling only occurring near the fin array base.

4.10. Conclusions

Pool boiling experiments at reduced pressures in water are conducted from an enhanced wavy-fin array. The pressures ranged from 1.0atm to 0.2atm. The reduction in pressure results in a performance lag with every surface. For the 145M8N-43 the performance lag is 12.5% at a heat flux of 145W/cm^2. The surface coating of fine wire mesh laminates proves to be an effective surface enhancement with the smaller pores and increased number of layers enhancing the performance the greatest. The 145M8N-43 surface which has the largest area enhancement factor (17) outperforms the 80M4N-43 surface by 10% at 145W/cm^2 and by 5% at 0.2atm. The increase in performance is due to the increase in the area enhancement factor from 12 to 17 and the increase in pore density for the two surfaces. In general, the larger the surface enhancement factor the more pores there are available to promote nucleation. This enhances the overall performance of the surface.

The semi-empirical model of the wavy-fin array is developed using a temperature dependent, correlation based heat transfer coefficient that is applied to the fin surface. This model calculates trends seen in the experimental data within an error of 30%. At 1.0atm and at a heat flux of 150W/cm^2 the model calculates an increase in superheat by

12.5%. The increase in superheat calculation is attributed to the fact that the model only takes into account the plane surface heat transfer coefficient and not the area enhancement of the wavy-fin. Assessment of the fin array effectiveness for increasing length shows that the plane surface is the most effective of the surface geometries. The 2.5mm tall array is more effective than the 5mm array. The heat transfer coefficient is large enough such that the height of the fin is inhibiting the amount of area that is at the base superheat. An advantage to the fin is that CHF for a given surface is delayed.

4.11. Appendix C: Nomenclature

A area [cm^2]

d wire filament diameter [mm]

D_h pore hydraulic diameter [μm]

D_{min} minimum bubble diameter due to surface tension-pressure force balance [m]

f bubble departure frequency [Hz]

g gravity

h heat transfer coefficient [W/m^2-K]

h_{fg} latent heat [kJ/kg]

k thermal conductivity [W/m-K]

L fin length [mm]

M mesh number [m^{-1}]

N number of layers [-]

n number of nucleation sites [-]

n''_{pores}	number of pores per unit area [m^{-2}]
P	pressure [atm]
Q	total heat flow [W]
q''	heat flux [W/cm^2]
Re	Reynolds number [-]
ΔT_{sat}	superheat, (T_w-T_{sat}) [K]
T	temperature [K]
x	location [mm]
z	location [mm]

Greek Symbols

β	specific surface area [cm^2/cm^3]
δ	laminate thickness [mm]
ε	porosity [-]
κ	number of pores with sufficient superheat for nucleation [-]
θ	Dimensionless Temperature $(T-T_{sat})/(T_b-T_{sat})$ [-]
η	Dimensionless Distance x/L [-]
μ	dynamic viscosity [$N-s/m^2$]
ρ	density [kg/m^3]
σ	surface tension [N/m]

Subscripts

b	base
e	effective
ez	effective out-of-plane

f	liquid phase
g	gas phase
h	pore hydraulic diameter
p	pool
sat	saturation

References

1. Mahajan, R., R. Nair, V. Wakharkar, J. Swan, J. Tang and G. Vandentop", Emerging Directions for Packaging Technologies", Intel Technology Journal, Vol. 6, pp. 62 – 75, 2002.
2. Haley K. W. and J. W. Westwater, "Boiling Heat Transfer From Single Fins", Proc. of the Int. Heat Trans. Conf., Vol. 3, pp. 245 – 253, 1966.
3. Webb R. L., "Donald Q. Kern Lecture Award Paper: Odyssey of the Enhanced Boiling Surface," Journal of Heat Transfer, vol. 126, Dec. 2004, pp. 1051-1059.
4. McGillis W. R. and V.P. Carey, "Pool Boiling Enhancement Techniques for Water at Low Pressure", Seventh Annual IEEE Semiconductor Thermal Measurement and Management Symposium: Feb. 12-14, 1991.
5. Nakayama, W., T. Nakajima and S. Hirasawa, "Heat Sink Studs Having Enhanced Boiling Surfaces for Cooling of Microelectronic Components", ASME Paper, 84-WA/HT-89, 1984.
6. Laca, P. and R.A. Wirtz, "Sub-Atmospheric Pressure Pool Boiling of Water on a Screen Laminate-Enhanced Extended Surface," 25th Annual Thermal Measurement, Modeling and Management Symposium, San Jose, CA, March 15-19, 2009

7. Jakob, M., Heat Transfer, Wiley, John and Sons, 1949
8. Gerlach, D. W. and Y. K. Yoshi, " Boiling Performance of Flourinert PF 5060 on Confined and Unconfined Wire Meshes Soldered to the Substrate", 2005 ASME International Mechanical Engineering Congress and Exposition, Nov. 5-11, 2005.
9. Li, C. and G.P. Peterson, "Parametric Study of Pool Boiling on Horizontal Highly Conductive Microporous Coated Surfaces", ASME JHT, Vol. 129, pp. 1465 – 1475, 2007.
10. Holland, B, Ozman, N and Wirtz, R.A., "Flow boiling of FC-72 from a screen laminate extended surface matrix", Microelectronics Journal, Vol. 38, pp. 1001 – 1007, 2008.
11. Sloan, A.D., Penley, S.J., and Wirtz, R.A., "Sub-Atmospheric Pressure Pool Boiling of Water on a Screen-Laminate Enhanced surface," 25th Annual Thermal Measurement, Modeling and Management Symposium, San Jose, CA, March 15-19, 2009
12. Penley, S.J. and Wirtz, R.A., "Correlation of Sub-atmospheric Pressure, Saturated, Pool Boiling of Water on a Structured-Porous Surface," ASME Journal of Heat Transfer, To Appear, 2010
13. Pal, A. and Y. Joshi, "Boiling of Water at Sub-Atmospheric Conditions With Enhanced Structures", 2005 ASME Summer Heat Transfer Conference, July 17-22, 2005.

14. Choon, N. G., A. Chakraborty, S.M. Aye, and W. Xiaolin, " New Pool Boiling Data for Water with Copper-Foam Metal at Sub-Atmospheric Pressures: Experiments and Correlation", Applied Thermal Engineering, Vol. 26, pp. 1286-1290, 2006.
15. Li, C., Z. Wang, P.I. Wang, Y. Peles, N. Koratkar, and G.P. Peterson, "Nanostructured Copper Interfaces for Enhanced Boiling", Small, Vol. 4, No. 8, pp. 1084-1088, 2008.
16. Xu, J., and Wirtz, R.A., "In-plane effective thermal conductivity of plain-weave screen laminates," Components and Packaging Technologies, IEEE Transactions on, 25(4), pp. 615 – 620, 2002
17. Kandlikar, S. et al., "Bubble nucleation and growth characteristics in subcooled flow boiling of water", ASME HTD-Vol. 342, National Heat Transfer Conference, pp. 11 – 18, 1997.
18. Steinke, M.E. and S.G. Kandlikar, "Control and effect of dissolved air in water during flow boiling in microchannels," International Journal of Heat and Mass Transfer, vol. 47, pp. 1925-1935, 2004.
19. Moffat, R.J., "Describing the Uncertainties in Experimental Results," Experimantal Thermal and Fluid Sciences, Vol 1, pp 3-17, 1988
20. Bayazit, B. B., K. D. Hollingsworth and L.C. Witte, " Heat Transfer Enhancement Caused by Sliding Bubbles," ASME JHT, Vol 25, pp. 503- 509, 2003.
21. Pioro I.L., W. Rohsenow and S.S. Doerffer, "I: review of parametric effects of boiling surface," International Heat and Mass Transfer, Vol. 47, pp. 5033–5044, 2004

22. Cole, R. and Rosenhow, W. M., "Correlation of bubble departure diameters for boiling of saturated liquids," Chemical Engineering Progress Symposium Series, 65(92), pp. 211-213, 1969

23. Nishikawa, K., Ito, T., and Tanaka, K., “Augmented Heat Transfer by Nucleate Boiling at Prepared Surfaces,” Proceedings ASME/JSME Thermal Engineering Conference 1, pp. 387-393, 1983

24. Mills, A.F., *Heat Transfer*, 2nd ed., Prentice Hall, NJ 1999